Toward Solar Fuels: Photocatalytic Conversion of Carbon Dioxide to Hydrocarbons

Somnath C. Roy,[†] Oomman K. Varghese,[†] Maggie Paulose, and Craig A. Grimes*

Department of Electrical Engineering, and Materials Research Institute, The Pennsylvania State University, University Park, Pennsylvania 16802. [†]These authors contributed equally to this work.

REVIEW

ABSTRACT The past several decades have seen a significant rise in atmospheric carbon dioxide levels resulting from the combustion of hydrocarbon fuels. A solar energy based technology to recycle carbon dioxide into readily transportable hydrocarbon fuel (*i.e.*, a solar fuel) would help reduce atmospheric CO_2 levels and partly fulfill energy demands within the present hydrocarbon based fuel infrastructure. We review the present status of carbon dioxide conversion techniques, with particular attention to a recently developed photocatalytic process to convert carbon dioxide and water vapor into hydrocarbon fuels using sunlight.

KEYWORDS: carbon dioxide recycling · global warming · photocatalytic conversion · TiO_2 nanotube array · electrochemical anodization · hydrocarbon fuels · gas chromatography

Hydrocarbon fuels are currently the most important source of energy due to their ready availability, stability, and high energy density (33 GJ/m^3 for gasoline).[1] In the United States, in 2008, hydrocarbon fuels (petroleum, natural gas, and coal) provided more than 80% of the energy.[1] Advantages such as being freely provided by Nature, high energy content, and ease of transportation and storage continue to drive our hydrocarbon dependence. Unfortunately, hydrocarbon fuel combustion carries with it the significant drawback of environmental pollution, to include carbon dioxide emissions,[2] and the associated impact on health that is generally not reflected in their purchase price.[3]

While volcano eruptions can demonstrate climate altering affects almost immediately, another less dramatic path to altering the earth's climate is to change the heat trapping properties of the atmosphere. It is well-established that higher atmospheric carbon dioxide (CO_2) levels result in an atmosphere that better retains heat. As such, atmospheric CO_2 plays a significant role in global heating appearing to act as the boundary condition, that is, the rule setter, as to what climates are available to the planet.[4] At the current rate of increase in atmospheric CO_2 concentration, many climate simulations suggest that the average global temperature will increase some 6 °C long before the end of the current century.[5] In a seminal work, Hansen and co-workers[6,7] use paleoclimate data to show that an average global temperature change of 6 °C is sufficient to swing earth's climate from one of glacial conditions to one supporting an ice-free Antarctica. A global cooling trend that began 50 million years ago is tied to falling CO_2 levels, with the planet being nearly ice-free until atmospheric CO_2 concentrations drop below 450 ± 100 ppm. A planet so hot as to make Antarctica ice-free must be warm indeed, presenting the possibility that vast regions of arable land that now sustain the worlds population may likely be given over to desert.[8] With a 2008 atmospheric CO_2 level of 385 ppm, business as usual with respect to hydrocarbon fuel use poses a suite of disconcerting issues.[9]

It has been suggested that CO_2 collected from emission sources may be stored in geological formations including oil and gas reservoirs, unminable coal seams, and deep sea reservoirs.[10] The strategy is the following: CO_2 emitted from point sources, such as coal-fired power plants, is trapped, purified, and then compressed for transportation to storage sites where it is injected into one geological formation or another. Of course, each of these steps—separation, purification, compression, transportation, and storage—requires additional energy. To maintain a constant power output given carbon capture and storage (CCS), studies have estimated that CCS equipped power plants would require an additional fuel input of 25 to 80%.[11−14] House and coworkers[15] report that the energy cost of capturing and storing 80% of the CO_2

*Address correspondence to cgrimes@engr.psu.edu.

Published online February 8, 2010.
10.1021/nn9015423

emitted from the U.S.'s 1493 coal-fired power plants, representing a power generation capacity of 336 GW, will require an additional 69−92 GW of CO_2-free base-load power, or a 15−20% reduction in overall electricity use.[15] Independent of the energy required to bury the CO_2 is the question of carbon sequestration leakage rates, rates which are likely to be more than zero. It is worth noting that in 1986 a burst of naturally sequestered carbon dioxide rose from Lake Nyos in Cameroon and asphyxiated 1700 people.[16]

VOCABULARY: **hydrocarbon fuels** – organic compounds consisting of carbon and hydrogen, such as gasoline, which currently serve as our most important source of fuel and energy due to their high energy content and relative stability · **photocatalytic reaction** – a catalytic process in which the catalysts are activated by photons or light radiation (such as UV light or solar radiation) of a suitable wavelength for generating electron−hole pairs that initiates chemical reactions · **gas chromatography** – an experimental technique used in analytical chemistry for the separation and analysis of different components in a gas mixture without decomposition · **electrochemical anodization of metal** – a process used in electrochemistry in which the metal electrode connected to the positive terminal (anode) of an electrochemical cell is simultaneously oxidized and etched, with nonporous oxide structures formed on the surface · **carbon dioxide reduction** – conversion of carbon dioxide to more useful chemicals such as hydrocarbons or synthesis gas by reacting it with hydrogen/hydrogen-containing compounds

As depicted in Figure 1, our interest is in the efficient recycling of CO_2 from a waste combustion product into a hydrocarbon fuel—a fuel that can be used within the current energy infrastructure, by use of sunlight. CO_2 is a stable molecule, and energy is required to convert it; hence CO_2 conversion makes sense only if the input energy is from a renewable source such as sunlight. Such solar fuels offer a ready means of storing and readily transporting solar energy.

DISCUSSION

CO_2 Conversion. ***Using Biomass.*** Biomass to fuel conversion is a viable approach for carbon recycling.[17,18] The basic process involves biomass production *via* photosynthesis, conversion of biomass into fuels such as ethanol or biodiesel using biochemical processes, and use of the bioresidue for production of biogas (methane). A variety of feedstocks are being used for biofuel production.

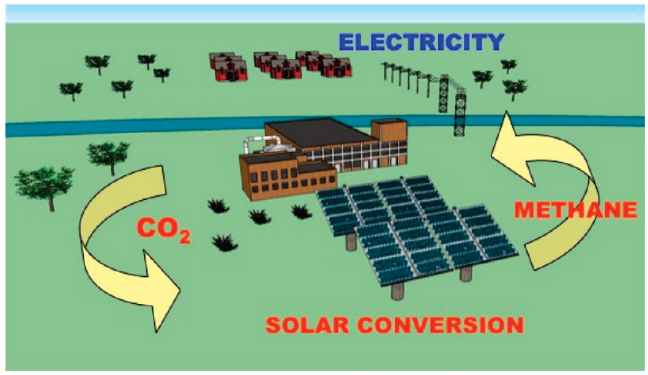

Figure 1. Depiction of integrated solar fuels system, where sunlight is used to convert CO_2 and water vapor into hydrocarbon fuels. Such fuels can be stored or transported as needed and, when used, result in CO_2 formation that is then passed to the photocatalytic array where it is converted back to fuel.

Bioethanol is commonly produced from sugar or starchy crops such as sugar cane and from plant cellulose using fermentation processes.[19] Biodiesel is produced from oil crops such as corn, soybean, jatropha, canola, coconut, oil palm, *etc.* or using microalgae.[20,21] Oil extracted from crops or microalgae *via* chemical or mechanical methods is subjected to a transesterification process to form alkyl esters (biodiesel). A typical transesterification process involves reaction of oil triglycerides with methanol in the presence of catalysts such as sodium hydroxide or potassium hydroxide (acids and lipase enzymes can also be used as catalysts) to form glycerol and methyl ester.[2] Biofuels are generally blended with petrodiesel for use in combustion processes.

Use of microalgae appears the most promising route to biofuel production. The oil content of algae is significantly higher than that of crops. Most algal species have a dry weight oil content of more than 30%,[17,21] while the oil content can go as high as 80% in some strains like *Schizochytrium* sp. and *Botryococcus braunii*.[17] Algae do not require arable land or fresh water for growth and fixes carbon dioxide at roughly 1.8 times its weight, facilitating carbon recycling.[22,23] If biodiesel is to be a significant source of global energy, it should be produced from microalgae.

Although world fuel production from biomass is rapidly increasing (3.91 quadrillion Btu from biomass in 2008, Department of Energy statistics), the sunlight-to-fuel energy conversion efficiency of photosynthesis is approximately 1%,[4,24] and other energy inputs required for biomass processing lower the overall sunlight to biofuel conversion efficiency. Therefore, tremendous land/water areas will be required for biomass to meet the energy needs of a developed country. Further, such massive cultivation of a single biological species will undoubtedly raise environmental challenges. It appears that biofuels will be a part of the future energy infrastructure but are unlikely to have a decisive role.[25]

Thermochemical. Artificial methods of carbon dioxide recycling involve retrieving CO_2 from the atmosphere or a point source, subjecting it to one or more chemical processes known for converting CO_2 into value added products, using these products for energy production and then capturing the released carbon dioxide to complete the cycle. External energy is required for CO_2 capture and conversion. Although various physical methods can also be employed, the process is primarily done chemically by absorbing CO_2 using solid or liquid phase (mono- or diethanolamine, potassium or calcium hydroxide, *etc.*) absorbents and regenerating them by supplying energy.[26,27] CO_2 conversion to CO or hydrocarbons is much more energy intensive, hence there is a critical need to obtain the required processing energy and hydrogen from renewable sources.

In this respect, hydrogenation of CO_2 over catalytic beds at elevated temperatures and pressures to make

hydrocarbons such as methane, or oxygenated hydrocarbons like methanol, is a viable approach if the hydrogen is derived from sunlight-driven water electrolysis and the process energy is supplied by solar panels.[28−31] Another strategy is to couple the reverse gas shift reaction with hydrogenation to form methanol or dimethyl ether.[26] Although not yet fully developed, direct reduction of carbon dioxide using concentrated sunlight *via* thermochemical cycles is one of the most promising approaches as it needs only CO_2, and water if hydrocarbons are to be synthesized, as feed stock. The process is tailored to generate carbon monoxide which can be combined with H_2, which needs to be generated *via* a renewable means, to make synthesis gas (syngas) which are in turn used as a fuel or feedstock for various processes including the Fischer−Tropsch for liquid hydrocarbon synthesis. Combining the thermochemical CO_2 and water splitting processes to synthesize hydrocarbons directly is an attractive alternative.

A one-step thermochemical process involves direct decomposition of CO_2 to carbon monoxide and oxygen.

$$CO_2 + \text{energy} \rightarrow CO + {}^1/_2O_2 \qquad (1)$$

The reaction is endothermic, and it involves a free energy change (ΔG^0) of 257 kJ/mol. For a 100% conversion of CO_2, the reaction should be carried at a minimum temperature of about 3075 °C,[32] at which ΔG^0 becomes zero. However, in principle, the CO yield can be as high as 30% at temperatures near 2400 °C,[33] although the yield is realistically much lower due to back reactions; quick product separation is essential to enhance the yield. Traynor and Jenson built a reactor for carrying out direct photolysis of CO_2 at high temperatures created by concentrated solar radiation (5000 suns) and achieved a CO yield of 6% and a solar to chemical energy conversion efficiency of 5%.[34] To make use of high temperature visible and infrared absorption properties of CO_2 in its splitting and thereby enhancing the efficiency, the CO_2 was preheated to about 1900 °C prior to its exposure to concentrated light. Pyrolysis and photolysis of CO_2 to CO occurred upon photon absorption, with the product gas stream rapidly cooled to quench the back reactions. However, product separation is a major problem in such single-step processes.

The reaction temperature can be significantly reduced and product separation achieved with multistep thermochemical cycles, as demonstrated through the development of multistep cycles for water splitting.[35] While discussing their concept of using a silver/silver halide cycle for water splitting by means of nuclear reactor heat Dorner and Keller proposed, probably for the first time, use of thermochemical closed cycles for CO_2 splitting as a way of environmental carbon mitigation.[36] Possibilities of using different multistep thermochemical cycles such as those based on cadmium, antimony, zinc, iron, and nickel for CO_2 conversion were discussed by Martin.[32] The thermodynamic calculations showed an efficiency advantage in using the Zn/ZnO cycle directly for carbon dioxide reduction rather than combining a water−gas shift reaction with a water splitting Zn/ZnO cycle to generate CO.

Galvez *et al.* carried out a second law thermodynamic analysis of Zn/ZnO and FeO/Fe_3O_4 cycles.[33] For example, the Zn/ZnO cycle is given by

$$ZnO \leftrightarrow Zn + {}^1/_2O_2 \qquad (2)$$

$$\Delta H^0_{25°C} = +350.5 \text{ kJ/mol}$$

$$Zn + CO_2 \leftrightarrow ZnO + CO \qquad (3)$$

$$\Delta H^0_{25°C} = -67.5 \text{ kJ/mol}$$

Reaction 2 is highly endothermic and requires a temperature of about 1700 °C to form gas phase zinc and oxygen. O_2 can be separated after reaction 2, and hence only CO is produced after reaction 3. Reaction 3 is exothermic, and an operating temperature between 425 and 725 °C is suggested. An efficiency of 39% is estimated on carrying out reaction 2 under concentrated solar radiation (5000 suns). Bamberger and Robinson reported experimental results of a cycle based on CeO_2.[37] CO_2 was reacted with Na_3PO_4 at 0−80 °C to form $NaHCO_3$, and CeO_2 was reacted with $Na_4P_2O_7$ at 850−950 °C to form $Na_2Ce(PO_4)_2$. The products of the two reactions, $NaHCO_3$ and $Na_2Ce(PO_4)_2$, were treated at 750−900 °C to form CO. Sandia National Laboratory is developing a two-step FeO/Fe_3O_4 thermochemical process, named "Sunshine-to-Petrol", to integrate CO_2 and H_2O splitting processes and make directly gasoline, diesel, or jet fuel as an end product.[26,38] It utilizes the concept of a thermochemical "heat engine" called Counter-Rotating Ring Receiver Reactor Recuperator (CR-5) to convert concentrated solar energy into thermal energy.[38] However, a number of materials challenges associated with high temperature operation in a reactive environment need to be solved for its development. Despite these isolated efforts and excellent ideas, thermochemical CO_2 splitting has yet to prove its viability.

Electrochemical. Following the concept of water electrolysis, a number of studies have examined the use of electrocatalysts to split CO_2 dissolved in liquids. A wide range of products starting from CO to more complex pure and oxygenated hydrocarbons of high energy content can be directly synthesized. Other prime advantages of this method include its compatibility with well-established water electrolysis technology and the possibility of using photovoltaic derived electricity, that is, a solar cell driven CO_2 electrolyzer, as work input. In general, the process involves electrolysis of a solution containing dissolved carbon dioxide; that is, carrying out the reduction of CO_2 by applying a voltage greater than that necessitated by thermodyamics between two

immersed electrodes. The standard redox voltage per electron for carbon dioxide splitting (given by reaction 1) is 1.33 V at 25 °C and 1 atm. The thermoneutral voltage is about 1.47 V, which is nearly same as that for water electrolysis. When the electrode overvoltages and Ohmic losses are added to thermoneutral voltage, a cell voltage of about 2 V or more is generally required to drive the reaction in aqueous electrolytes.[39,40]

In aqueous electrolytes such as $NaHCO_3$ and $KHCO_3$, water and carbon dioxide reduction processes take place simultaneously at the cathode due to the proximity of their reduction potentials (H^+/H_2O potential is -0.41 V *vs* NHE whereas CO/CO_2 potential is -0.52 V *vs* NHE at pH = 7). While this is an advantage for the production of a wide range of hydrocarbons by co-electrolysis of water and carbon dioxide, thermodynamic preference on hydrogen generation over CO_2 reduction lowers the Faradaic efficiency for carbon dioxide reduction unless hydrogen evolution is suppressed. Note that only dissolved CO_2 undergoes reduction and ions in the electrolyte are not consumed.[41,42] The types of products formed and the Faradaic efficiencies of their formation depend upon various factors, primarily catalytic activity of the electrodes, potentials applied to the electrodes, type of ionic species in the electrolyte, and local pH and CO_2 concentration near the electrode that are determined by buffer strength, mass transport, and bulk CO_2 concentration in the electrolyte.[43]

The electrode material has a major role in determining the products and selectivity. The crystal orientation (hence preferential adsorption of reactants and intermediates), surface structure (*e.g.*, roughness, porosity, and defects), surface crystallography (dislocations and vacancies), surface impurities, and electronic configuration (*e.g.*, sp and d metals) are important factors determining the catalytic activity of a particular material.[43−49] Hydrogen evolution dominates over hydrocarbon generation in the case of Pt, Ni, Ti, Co, Rh, Ir, and Fe electrodes due to their low hydrogen overpotentials and strong CO adsorption characteristics.[40,43,47,50] Metals such as Hg, Cd, Pb, Sn, Tl, In, and Bi do not necessarily split CO_2, hence formate ions are primarily generated.[43,50,51] Negligible CO adsorption and high hydrogen overpotentials make them poor catalysts for CO_2 reduction. Metals such as Au, Ag, Pd, Ga, Cu, and Zn have moderate hydrogen overvoltage and weak CO_2 adsorption characteristics. While CO evolution is promoted in most of these materials, Cu facilitates reaction of CO and H_2 to generate hydrocarbons, aldehydes, and alcohols as major products.[43,52,53] Of the various materials investigated as electrocatalysts, copper has been considered one of the most appropriate materials for the production of hydrocarbons and oxygenated hydrocarbons in aqueous solutions.[47] Copper deactivation is a commonly observed problem, but ways to alleviate this have been proposed.[54] Alloys like Cu−Zn, Raney Fe−Ru/C, Pt−Pd−Rh, Ru−Pd, and conducting polymers like polyaniline have also been investigated for their electrocatalytic activity for CO_2 reduction.[55−59]

While generally C1 hydrocarbons, that is, hydrocarbon chains with one carbon atom, are formed in aqueous electrolytes, there are instances of formation of larger hydrocarbon chains. A Cu electrode, not electropolished, yielded up to C6 hydrocarbons including paraffins and olefins with ethylene as the major component.[45] Surface oxygen coverage, promoted by the surface crystallinity, was believed to be an important factor controlling the CO_2 activation selectivity.[43,45] Centi *et al.* demonstrated that carrying out gas phase reaction in an electrochemical cell employing nanocarbon based electrocatalysts and a proton exchange membrane (PEM) would produce hydrocarbons and alcohols with chains having up to 10 carbon atoms.[48] They obtained isopropyl alcohol as the primary product with ethanol, methanol, acetaldehyde, and acetone at lower concentrations and trace amounts of alkanes and aromatics when electrocatalytic CO_2 reduction was performed at 60 °C in a cell with an Fe−Co/carbon nanotube based gas diffusion membrane electrode. Earlier, the same group had reported generation of primarily >C5 (chains with greater than 5 carbon atoms) compounds when the electrolysis was performed in a cell with similar configuration but at room temperature and using Pt nanoparticle on carbon black as electrodes, which were hot-pressed onto a Nafion membrane.[60] In their experiments, a cell with liquid electrolyte on one side (0.5 M $KHCO_3$) and gas phase (CO_2 + 4% H_2O) on the other side yielded a maximum rate of formation of >C7 hydrocarbons. Hori *et al.* observed that Faradaic efficiency for methane formation dropped from about 65% to almost 0 while that for ethylene formation increased from 0 to 20% when the temperature was increased from 0 to 40 °C.[61]

The reaction kinetics and product selectivity change with the potential applied to the electrode. For example, Noda *et al.*[62] reported that the Faradaic efficiencies of formation of $HCOO^-$, CO, C_2H_4, and CH_4 varied with electrode potential, for a potential in the range of -1.35 to -1.75 V (*vs* KCl saturated Ag/AgCl) applied to a copper electrode in $KHCO_3$ electrolyte. The maximum Faradaic efficiencies observed were 32% at -1.4 V for $HCOO^-$, 33% at -1.52 V for CO, 41% at -1.58 V for C_2H_4, and 39% at -1.7 V for CH_4. Oxygenated hydrocarbons such as ethanol, acetaldehyde, propanol, and propionaldehyde were also present at low concentrations, with Faradaic efficiencies that peaked between -1.57 and -1.65 V. The change seen in reactant formation from formate to hydrocarbons with a corresponding increase in negative potential was basically due to enhanced CO_2 reduction. However, hydrogen evolution increased substantially for a potential above -1.75 V (Faradaic efficiency >80%) with the formation of carbon based products sharply declining.

CO_2 concentration in the electrolyte and mass transport are decisive factors in determining the Faradaic formation efficiencies of the different products.[50] Reducing the electrolyte temperature enhances solubility as well as stability of the reduction intermediates, hence a temperature close to zero is generally chosen. However, while performing electrolysis at higher temperatures reduces CO_2 solubility, the relative selectivity to C1 products reduces and that to C2 products increases.[63] Increasing the pressure increases the solubility and in general improves the Faradaic efficiency for CO_2 reduction;[48,50] the relative formation efficiency of the different products also changes with pressure.[64] Ohta *et al.* used ultrasonic irradiation to enhance the mass transport near the electrode and suppress hydrogen formation.[65] Use of gas diffusion electrodes has also been found to improve mass transport and hence product formation rate and selectivity depending upon the electrode material.[50,66]

Because of the low solubility of CO_2 in aqueous solutions (33 mM at 25 °C at 1 atm CO_2), nonaqueous, particularly organic aprotic solvents, which can dissolve much more CO_2, are often used as electrolytes. Methanol, dimethyl formamide, dimethyl sulfoxide, acetonitrile, and propylene carbonate are examples of CO_2 solvents used as electrolytes.[67] In nonaqueous electrolytes, the solubility of CO_2 is high but poor solution conductivity leads to high Ohmic losses.[48,50] Methanol seems to be a better choice due to its moderate CO_2 solubility (5 times that of aqueous solutions) and Ohmic losses.[68−71] Nonaqueous electrolytes provide the ability to work below freezing point of water, and hence the benefit of increased solubility at low temperatures can be exploited. Further, hydrogen evolution is suppressed in nonaqueous solutions, especially at lower temperatures, and hence the possibility of increased current efficiency for CO_2 reduction. Compared to aqueous solutions, more complex compounds such as oxalic acid, glycoxylic acid, tartaric acid, *etc.* are formed in nonaqueous solutions.[49] Cu electrodes that form hydrocarbons in aqueous electrolytes primarily generate CO in nonaqueous electrolytes. Nevertheless, this scenario may change depending upon the hydrophobic/hydrophilic behavior of the cations.[50,72] Silver- and boron-doped diamond are considered promising electrode materials.[50]

A number of transition complexes, both metal based and ligand based complexes (photo/electrocatalysts), have also been investigated as catalysts with low overpotentials for CO_2 reduction. This includes metal complexes with macrocyclic ligands,[73,74] metal complexes with bipyridine ligands,[75] and transition metal phosphine complexes.[76] The metal complexes are either dissolved in the electrolyte medium to serve as redox mediators or deposited on a solid or gas diffusion electrode surface.[50,77] The electrocatalytic activity of the transition metal complexes is dependent on details of both the metal center and the ligand.[78]

Transition metal catalysts with macrocyclic ligands and tetraazo macrocyclic complexes of Co and Ni are able to reduce CO_2 to CO or a mixture of CO and atomic hydrogen at potentials ranging from −1.3 to 1.6 V *vs* SCE. These catalysts are also able to provide high current efficiencies; however, slower rates of regeneration and the formation of an insoluble compound layer in the presence of CO affect the long-term stability of these catalysts.[79] The use of Fe based complexes such as iron(0) porphyrins is able to reduce CO_2 in the presence of weak Brønsted acids, for example 1-propanol, and the catalytic process is significantly improved in terms of both the efficiency and turnover frequency; however, the required reduction potentials (≈−1.5 V *vs* SCE) are highly negative for practical purposes and also require the use of mercury electrodes.[80] In contrast to macrocyclic ligands, metal complexes with bipyridine ligands show excellent current efficiencies and much better selectivity for CO over hydrogen production; however, these systems show low turnover frequencies. Among the various metal complexes with phosphine ligands, binuclear Ni(0) complex $[Ni_2(CNMe)_3(dppm)_2][PF_6]_2$ offers low negative operating voltages (≈−0.87 V *vs* SCE); however, carbonyl formation occurs over extended periods of time.[81] Another binuclear complex $[Ni_2(\mu\text{-dppa})_2(\mu\text{-CNR})(CNR)_2]$ shows interesting catalytic behavior of trapping the reduction product CO that makes it the most suitable candidate for equilibrating CO_2 with its reduction products CO and CO_3^{2-}.[82] Benson *et al.* presented a comprehensive review on developments in this area.[83] Use of metal complex polymer composites,[84] and Fe, Pt-catalyzed carbon nanotubes[85] has also been reported.

Bouwman and co-workers recently reported spontaneous oxidation of a dinuclear copper(I) complex to oxalate by CO_2 in air.[86] The tetranuclear copper(II) oxalate complex formed after reaction with CO_2 in air was electrolyzed at −0.03 V *vs* NHE in CO_2 saturated acetonitrile solution containing lithium perchlorate to precipitate lithium oxalate. The solution, after removing the oxalate and saturating with argon, was subjected to a second electrolysis to return to the copper(I) complex. This method is promising as CO_2 is directly, and selectively, captured from air. Although it is not evident in this particular case, in general, the lack of stability is a major problem with metal complexes.

The feasibility of using water electrolyzer configurations, primarily with liquid electrolytes, solid polymer membrane, and solid oxide, for CO_2 reduction or combined CO_2 and H_2O splitting has been tested by various groups.[61,87−90] For example, Bidrawn *et al.* examined the use of a solid oxide electrolyzer fitted with a ceramic electrode based on $La_{0.8}Sr_{0.2}Cr_{0.5}Mn_{0.5}O_3$ infiltrated into a yttria-stabilized zirconia scaffold together

with 0.5 wt % Pd supported on 5 wt % $Ce_{0.48}Zr_{0.48}Y_{0.04}O_2$ for CO_2 reduction at temperatures in excess of 700 °C and demonstrated CO_2 reduction with an efficiency comparable to water splitting.[88] Zhan *et al.* produced syngas by co-electrolysis of steam and CO_2 using a solid oxide electrolyzer at 700−800 °C.[89]

Photo-Assisted Conversion of CO_2 to Hydrocarbon Fuels. Direct solar conversion of CO_2 and water vapor into hydrocarbon fuels using sunlight is an attractive prospect, serving to reduce atmospheric CO_2 concentrations while providing on a renewable basis an energy dense portable fuel compatible with our current energy infrastructure. As depicted in Figure 1, we suggest a strategy of using the fuel on a closed-loop basis; fuel is burned, the CO_2 emissions are collected and passed into a photocatalytic bed where solar energy is used to convert the CO_2 back into fuel. Of critical importance is the efficiency of the photocatalytic materials in their use of sunlight for conversion of CO_2 to fuel.

One of the earliest reports on photoelectrochemical reduction of carbon dioxide was published by Halmann in 1978.[91] An electrochemical cell was used, composed of a single crystal p-type GaP cathode, carbon anode, and a buffered aqueous electrolyte through which carbon dioxide was bubbled. When the GaP crystal was illuminated (mercury lamp) and a voltage bias applied, current was detected, with the electrolyte solution showing the presence of formic acid, formaldehyde, and methanol. Many research groups have since investigated the use of different compound semiconductors to achieve higher visible light catalytic activities. Using p-GaAs and p-InP photoelectrodes in a CO_2-saturated solution of Na_2SO_4, Canfield and Frese achieved CO_2 reduction to methanol.[92] Similarly, formation of methanol together with formic acid and formaldehyde was reported by Blazeni *et al.* using single-crystal p-GaP and p-GaAs photoanodes.[93] Eggins and co-workers reported visible light photoreduction of CO_2 in the presence of colloidal CdS in an aqueous solution of tetramethylammonium chloride, yielding glyoxylic acid as well as formic and acetic acids and CH_2O.[94] Fujiwara and co-workers studied the use of ZnS nanocrystals as visible light photocatalysts, finding that excess metal ions enhanced the photocatalytic response, a behavior attributed to the formation of sulfur vacancies that acted as catalytic sites for CO_2 reduction.[95] Use of ZnS crystallites was also reported by Kuwabata *et al.*, in which methanol was obtained as the main product.[96] Barton and co-workers reported selective reduction of CO_2 to methanol using a catalyzed p-GaP based photoelectrochemical cell.[97]

In 1979, Inoue and co-workers[98] examined the use of semiconductor powders for CO_2 reduction, including TiO_2, ZnO, CdS, SiC, and WO_3, suspended in CO_2-saturated water illuminated by a Xe lamp. Small amounts of formic acid, formaldehyde, methyl alcohol, and methane were produced. Inoue suggested that conversion of CO_2 to methane was a multistep reduction process given by

$$H_2O + 2h^+ \rightarrow {}^1/_2O_2 + 2H^+ \quad (4)$$

$$CO_2(aq.) + 2H^+ + 2e^- \rightarrow HCOOH \quad (5)$$

$$HCOOH + 2H^+ + 2e^- \rightarrow HCHO + H_2O \quad (6)$$

$$HCHO + 2H^+ + 2e^- \rightarrow CH_3OH \quad (7)$$

$$CH_3OH + 2H^+ + 2e^- \rightarrow CH_4 + H_2O \quad (8)$$

with e^- and h^+ denoting, respectively, photogenerated electrons and holes. The formaldehyde and methyl alcohol yield was highest in the presence of SiC, a behavior attributed to the relative position of the SiC conduction band with respect to the $HCHO/H_2CO_3$ redox potential.[98] Figure 2 shows a schematic of the band-edge positions of the different semiconductor materials with respect to the redox potentials of the different chemical species. The SiC conduction band edge lies at a higher position (more negative) than the $HCHO/H_2CO_3$ redox potential, which is believed to be responsible for the high rates of product formation. The absence of methyl alcohol when WO_3 was used as catalyst, with a conduction band at a position lower than the $HCHO/H_2CO_3$ redox potential, further indicates the influence of band-edge positions on CO_2 reduction.

In subsequent work, Halmann *et al.* reported the use of strontium titanate catalyst powder suspended in an aqueous solution through which CO_2 was bubbled, illuminated by natural sunlight to produce formic acid, formaldehyde, and methanol.[99] Due to its higher conduction band-edge position compared to the redox potential of CH_3OH/H_2CO_3, strontium titanate could effectively reduce carbon dioxide dissolved in an aqueous

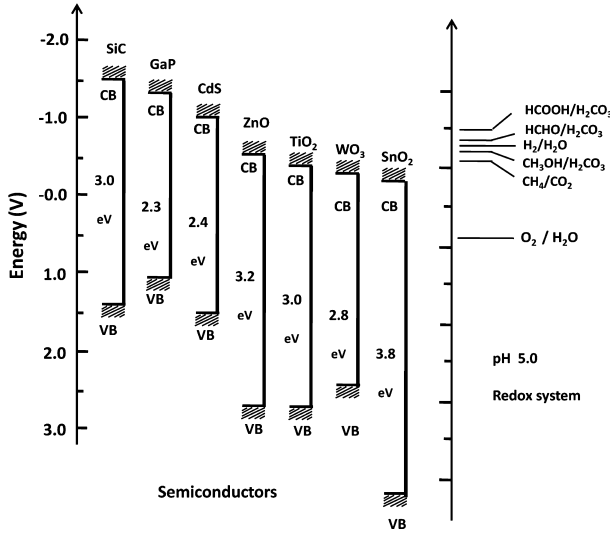

Figure 2. Conduction band and valence band potentials of semiconductor photocatalysts relative to energy levels of the redox couples in water. Reprinted with permission from ref 98. Copyright 1979 Macmillan Publisher Limited.

electrolyte. Cook and co-workers[100] using a mixture of *p*-SiC and Cu particles reported the reduction of CO_2 to CH_4, C_2H_4, and C_2H_6 as a function of electrolyte pH. Their work showed that the addition of Cu cocatalysts to SiC enhanced the electron transfer rate from the SiC conduction band, while CO_2 reduction occurred on the Cu particle sites. The use of Cu as a cocatalyst was also reported by Adachi *et al.*, in which Cu-loaded TiO_2 powder was suspended in a CO_2 pressurized solution at ambient temperature, with methane and ethylene produced under Xe lamp illumination.[101]

Anpo and Chiba reported the use of highly dispersed titanium oxide on glass for the photocatalytic reduction of carbon dioxide.[102] UV illumination of the catalyst in the presence of CO_2 and H_2O resulted in the photocatalytic formation of CH_4, CH_3OH, and CO as major products. From the direct detection of intermediate species, they proposed that methane formation resulted from the reaction between carbon radicals and atomic hydrogen, with the photoreaction efficiency strongly dependent upon the CO_2 to H_2O ratio and reaction temperature. The charge transfer excited state, $Ti^{3+}-O^-$ of the tetrahedral coordinated titanium oxide species, was found to play a critical role in determining the photoreactivity. The use of Cu as a cocatalyst in combination with TiO_2 resulted in methanol formation. In another report Anpo *et al.* examined photocatalytic reduction of CO_2 and water vapor at 328 K using titania-loaded zeolite, which demonstrated a high selectivity for gas phase methanol formation.[103] Addition of Pt to the TiO_2 led to an increased methane yield compared to methanol formation.[103]

Sayama and Arakawa reported use of 1% Cu-loaded ZrO_2 as a catalyst for photocatalytic reduction of CO_2 to CO in $NaHCO_3$ solutions under UV irradiation.[104] Using Ti-containing porous SiO_2 films, Ikeue *et al.* reported the formation of methane and methanol from a mixture of CO_2 and H_2O vapor under Hg lamp illumination.[105] Matsumoto *et al.* studied the use of p-type $CaFe_2O_4$ powder for CO_2 reduction in saturated NaOH solution;[106] under Hg lamp illumination, they obtained methanol and formaldehyde as the main products. Ichikawa and Doi reported a photoelectrocatalysis system comprising a thin film anatase TiO_2 layer on one side of a Nafion substrate and ZnO with Cu electrocatalysts on the other. Under illumination (mercury lamp, as well as sunlight), CO_2 was converted to hydrocarbons with methane and ethylene as the major products.[107] Guan *et al.* investigated the use of Pt-loaded $K_2Ti_6O_{13}$ catalysts for reduction of CO_2 in water under concentrated sunlight illumination.[108] They obtained methane, acetic acid, and acetaldehyde along with hydrogen. The inclusion of an additional catalyst, iron on a dealuminated Y-type zeolite (Fe−Cu−K/DAY), resulted in formation of methanol and ethanol in addition to the above species as dependent upon the reaction temperature. Recently, Sasirekha *et al.* reported photocatalytic production of methanol from CO_2 using Ru-doped TiO_2/SiO_2 catalysts;[109] maximum photocatalytic activity was obtained at an optimum concentration of 0.5% Ru and 10 wt % TiO_2 in SiO_2.

Ulagappam and Frei used Ti-silicalite molecular sieves as a catalyst for 266 nm UV laser radiation induced reduction of CO_2 and H_2O gas mixtures, obtaining HCO_2H, CO, and HCO_2CH_3.[110] Product origins were studied by IR spectroscopy, indicating that CO originated from the secondary photolysis of HCO_2H, while HCO_2CH_3 was the result of spontaneous Tishchenko reaction of $CH_2{=}O$.[110] In a subsequent work, Lin and co-workers carried out a detailed study of the photoinduced reduction of carbon dioxide in TiMCM-41 (Ti-substituted Mobile Catalytic Material No. 41) sieves using *in situ* FTIR spectroscopy at room temperature.[111] Carbon monoxide was observed as the sole product, with production rates linearly corresponding to laser power. Their study determined that CO production was a single-photon, two-electron transfer product of CO_2 with H_2O acting as an electron donor. In a recent report, Tan *et al.* investigated the photocatalytic reduction of CO_2 under monochromatic UV (253.7 nm) radiation in the presence of TiO_2 pellets soaked in water, obtaining a maximum rate of about 0.25 μmol/h of methane, 0.16 μmol/h of hydrogen, and trace amounts of CO.[112]

Lo and co-workers attempted CO_2 reduction using TiO_2 (Degussa, P-25) and ZrO_2 powder photocatalysts illuminated, respectively, with 264 and 365 nm UV radiation in the presence of hydrogen and water. Photoreduction of CO_2 over TiO_2 in the presence of $H_2 + H_2O$ yielded CH_4, CO, and C_2H_6, while the use of ZrO_2 with H_2 formed only CO.[113] Nishimura *et al.* used sol−gel derived TiO_2 multilayer films inside a Cu tube to obtain a total product (CO, CH_4, C_2H_4, and C_2H_6) formation rate of about 3.2 nmol/cm^2 · h under 2.4 mW/cm^2 UV illumination.[114] The use of TiO_2 in combination with multiwalled carbon nanotubes has been reported by Xia and co-workers to produce ethanol and formic acid through photocatalytic reduction of CO_2.[115] It was found that ethanol was the major resultant product when the composite catalyst was prepared by sol−gel, while formic acid was the major resultant product when the composite catalyst was prepared *via* a hydrothermal technique.[115] Wu *et al.* investigated the use of fine particle layers of TiO_2, Cu/TiO_2, and Ag/TiO_2 photocatalysts.[116] Moist CO_2 was photocatalytically reduced to methanol under UV irradiation; a maximum methanol production rate of 4.12 μmol/g · h was obtained with 1.0 wt % Ag-TiO_2 catalyst under 10 W/cm^2 UV radiation.[116]

Gratzel and co-workers[117] obtained selective production of methane from a mixture of CO_2 and H_2 in Ar using Ru/RuO_x sensitized TiO_2 particles. Figure 3 shows the production of methane in light and dark and the reduction of carbon dioxide with time.[117] An initial methane production rate of about 116 μL/h per 100 g of nanoparticles was obtained under simulated

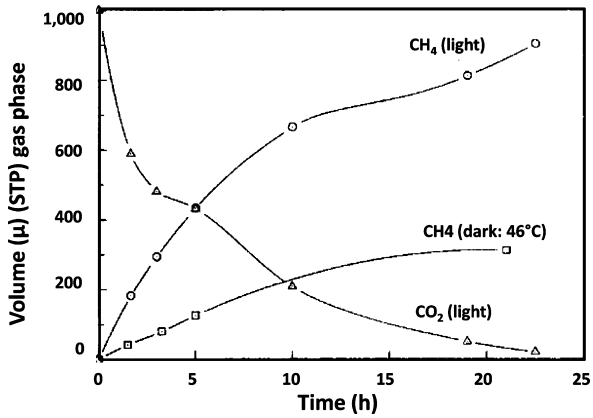

Figure 3. Photoconversion of CO_2 to CH_4. The decrease in CO_2 and increase in CH_4 volume is plotted as a function of illumination time. Reprinted with permission from ref 117. Copyright 1987 Macmillan Publisher Limited.

light. It was initially suggested that carbidic surface carbon (Ru−C) played a crucial role in CO_2 reduction using the TiO_2−Ru photocatalysts. Such Ru−C species were formed by the existence of isolated carbon atoms coordinated to Ru without the formation of graphitic islands or overlayers. Gratzel and co-workers proposed that the photogeneration of these Ru−C species involved band gap excitation of TiO_2 catalysts, followed by a Ru-assisted reduction of CO_2 by conduction band electrons according to the reaction

$$4e^- + CO_2 + \text{Ru(catalyst)} \rightarrow \text{Ru}-\text{C} + 2O^{2-} \quad (9)$$

with methane generated by the reaction of surface carbon with hydrogen:

$$\text{Ru}-\text{C} + 2H_2 \rightarrow \text{Ru} + CH_4 \quad (10)$$

However, after a comprehensive study, Melsheimer *et al.* concluded that the photocatalytic reduction of CO_2 over Ru-TiO_2 catalysts reported by Gratzel and co-workers did not involve intrinsic photochemical effects and was mainly due to thermal effects.[118] They suggested that the localized Ti^{3+} states were responsible for the sensitization of the catalytic support, which led to conversion of visible light into heat and a corresponding increase in CO_2 reduction.

Metal complexes involving rare-earth elements have also been used by many research groups for the photocatalytic CO_2 reduction. Takeda *et al.* reported the use of rhenium complex in a dimethyl formamide (DMF) solution for the reduction of CO_2 to CO.[119] Lehn and Ziessel examined reduction of CO_2 within an acetonitrile/water/triethylamine mixture using a Ru(2,2′-bipyridine)$_3^{2+}$ cobalt(II) chloride catalyst under visible light illumination.[120] In preference to water reduction, a higher selectivity for CO_2 reduction to CO was achieved when triethanolamine was used instead of triethylamine. Craig *et al.* reported the use of photosensitizer Ru(bpy)′$^{+}$ (bpy = 2,2′-bipyridine) in an ascorbate-buffered solution at room temperature under 1 atm of carbon dioxide in the presence of nickel(II) complexes, either Ni[1,4,8,11-tetraazacyclotetradecane] or Ni[1,4,7,10-tetraazacyclododecane], with the reduction of CO_2 to formate and CO.[121] Early developments in the field of photochemical carbon dioxide reduction using various metal complexes have been summarized in a review by Fujita.[122] Recently, Gholamkhass and co-workers reported the investigation of ruthenium−rhenium bi- and tetranuclear complexes for photocatalytic CO_2 reduction.[123] Ozcan *et al.* sensitized a Pt/TiO_2 catalyst with tris(2,2′-bipyridyl)ruthenium(II) chloride hexahydrate dye, obtaining enhanced visible light activity toward methane production *via* CO_2 reduction.[124] However, these high-cost metal complexes suffer from poor stability particularly when exposed to UV light.

A summary of some of the important works in this field are presented in Table 1. In the majority of the noted reports, CO_2 reduction was achieved in an electrochemical cell requiring electrical bias and/or UV illumination. The energy associated with the electrical bias, and the UV light source, if not provided on a renewable basis, clearly offsets any advantage inherent to CO_2 conversion. What we seek is a means for achieving high-rate photocatalytic reduction of carbon dioxide, using as the only input energy source solar radiation. Since visible light comprises the majority of the solar spectrum energy, it behooves us to consider photocatalysts sensitive to sunlight.

Photocatalytic Conversion of CO_2 Using Nitrogen Doped TiO_2 Nanotube Arrays. A significant breakthrough in the photocatalytic reduction of gas phase CO_2 by solar radiation has recently been achieved by Varghese and co-workers, using nitrogen-doped TiO_2 nanotube arrays cocatalyzed with copper and/or Pt nanoparticles, in which water vapor saturated carbon dioxide was reduced to methane and other hydrocarbons without application of an electrical bias.[125] The nanotube array architecture, see Figure 4, offers large surface areas and wall thicknesses of a few nanometers, facilitating efficient charge separation while the columnar shape of the tubes enables directed (vectorial) charge transfer. TiO_2 nanotube arrays formed by anodic oxidation have found application as high-precision self-cleaning gas sensors,[126−128] use as photoanodes for hydrogen production *via* water photoelectrolysis,[129−131] as the electron transporting backbone in dye-sensitized as well as heterojunction solar cells,[132−136] and as a biocompatible material for enhanced osseointegration.[137−140]

Vertically oriented n-type TiO_2 nanotube arrays, see Figure 4, directly achieved by Ti anodization, have been shown to possess outstanding photocatalytic properties.[141] The walls of the crystallized nanotubes consist of stacked anatase crystallites that provide facile pathways for photogenerated carrier transport. The nanotube array structure makes available to the reactant gas species both sides of the tube walls, that is, inner and

TABLE 1. Summary of Some Important Reports on Photocatalytic Reduction of CO_2 (Efficiency Values for a Few Selected Results Are Also Given)

light source	catalyst	reaction medium	products	efficiency	reference
mercury (Hg) lamp	*p*-GaP single crystal	CO_2-saturated buffered solution (electrochemical cell)	formic acid, formaldehyde, methanol	$\eta = 0.61\%$ (for methanol)	Halmann, ref 91
tungsten−halogen lamp	*p*-GaAs, *p*-InP	CO_2-saturated Na_2SO_4 (EC cell)	methanol	faradaic eff. = 0.52 (*p*-GaAs)	Canfield and Frese, ref 92
xenon (Xe) lamp	*p*-GaAs, *p*-GaP single crystal	CO_2 saturated aqueous solution (EC cell)	methanol, formic acid, formaldehyde	FE = 0.8 (max.)	Blajeni *et al.*, ref 93
visible light 320−580 nm	colloidal CdS	aqueous solution of tetramethylammonium chloride	glyoxylic acid, formic and acetic acid	QE = 0.00125%	Eggins *et al.*, ref 94
Hg lamp	ZnS nanocrytals	dimethylformamide solution with distilled triethylamine	formic acid		Fujiwara *et al.*, ref 95
UV Hg lamp	ZnS microcrystals	$NaHCO_3$ and K_2HPO_4 solution	methanol	QE = 5.9%	Kuwabata *et al.*, ref 96
UV 365 nm	*p*-GaP	EC cell	methanol	$\eta = 10.9\%$, QE = 44% at −0.5 V	Barton *et al.*, ref 97
UV Xe lamp	SiC and other semiconducting powders	EC cell	methanol, formic acid, formaldehyde, methane		Inoue *et al.*, ref 98
natural sunlight through solar concentrator	$SrTiO_3$ powder	aqueous suspension	formic acid, formaldehyde, methanol	$\eta = 0.011\%$	Halmann *et al.*, ref 99
UV 365 nm	Cu added p-SiC	$KHCO_3$ solution	methane, ethane, and ethylene		Cook *et al.*, ref 100
UV Xe lamp	Cu added TiO_2	aqueous suspension with pressurized CO_2	methane, ethylene		Adachi *et al.*, ref 101
UV Hg lamp	TiO_2 loaded zeolite	CO_2 and H_2O vapor	methanol		Anpo *et al.*, ref 103
UV Hg lamp	Cu added ZrO_2	$NaHCO_3$ solution	CO		Sayama and Arakawa, ref 104
UV Hg lamp	Ti containing SiO_2 film	CO_2 and H_2O vapor	methane and methanol	QE = 0.28%	Ikeue *et al.*, ref 105
UV laser 266 nm	Ti-silicalite molecular sieve	CO_2 and H_2O vapor	CO, formaldehyde, acetaldehyde		Ulagappam and Frei, ref 110
UV lamp	TiO_2 powder	CO_2 and H_2O vapor	methane, hydrogen, CO		Tan *et al.*, ref 112
UV lamp	TiO_2 (Degussa, P25), ZrO_2	$H_2 + H_2O$	methane, ethane, CO		Lo *et al.*, ref 113
UV 365 nm	MW-CNT supported TiO_2	CO_2 and H_2O vapor	ethanol, formic acid		Xia *et al.*, ref 115
UV 365 nm	Ag/Cu-TiO_2 coated optical fiber	CO_2 and H_2O vapor	methanol	QE = 0.00013%	Wu *et al.*, ref 116
UV 310−435 nm	Ru/RuO_x sensitized TiO_2	CO_2, H_2 in Ar	methane		Thampi *et al.*, ref 117
Hg arc lamp $\lambda >$ 330 nm	Rh complex	CO_2 bubbled through DMF-TEOA solution	CO	QE = 0.59%	Takeda *et al.*, ref 119
visible light $\lambda >$ 400 nm	Ru-bipyridine-Co(II) chloride	acetonitrile/water/ triethyleamine	CO		Lehn and Ziessel, ref 120
natural sunlight of AM 1.5 illumination	Cu, Pt cocatalyzed N-doped TiO_2 nanotube arrays	CO_2 and H_2O vapor	methane, other alkanes, olefins, Br-paraffins, H_2, CO.	$\eta = 0.0148\%$, QE = 0.74%	Varghese *et al.*, ref 125
visible light $\lambda >$ 420 nm	CdSe/Pt/TiO_2 heterostructure	CO_2 and H_2O vapor	methane, methanol, CO, H_2		Wang *et al.*, ref 158

outer surfaces, for enhanced photocatalytic reactions. The hole diffusion length in titania is ≈10 nm,[142] and the electron diffusion length has been reported as high as ≈100 μm,[143] while half of the nanotube wall thickness is approximately 10 nm. The high rate of carbon dioxide conversion can be attributed to the high surface area and nanoscale wall thickness of the nanotubes, enabling the surface species to readily receive both charge carriers generated near the surface due to the wave function overlap and those generated deep inside the wall *via* diffusion. Since half of the nanotube wall thickness is less than or comparable to the minority carrier (hole) diffusion length, both holes and electrons are never generated far from the semiconductor−reactant gas interface. Therefore, irrespective of the nanotube length, charge carriers generated deep inside the nanotube walls reach the interface by diffusion, while charge carriers created near the interface region are readily accessible to the reactant species. Hence without compromising the enhanced photocatalytic properties, we are able to increase the nanotube length, facilitating light absorption, including utilization of weakly absorbed wavelengths, for photocatalytic processes. Furthermore, any loss due to reflection of the in-

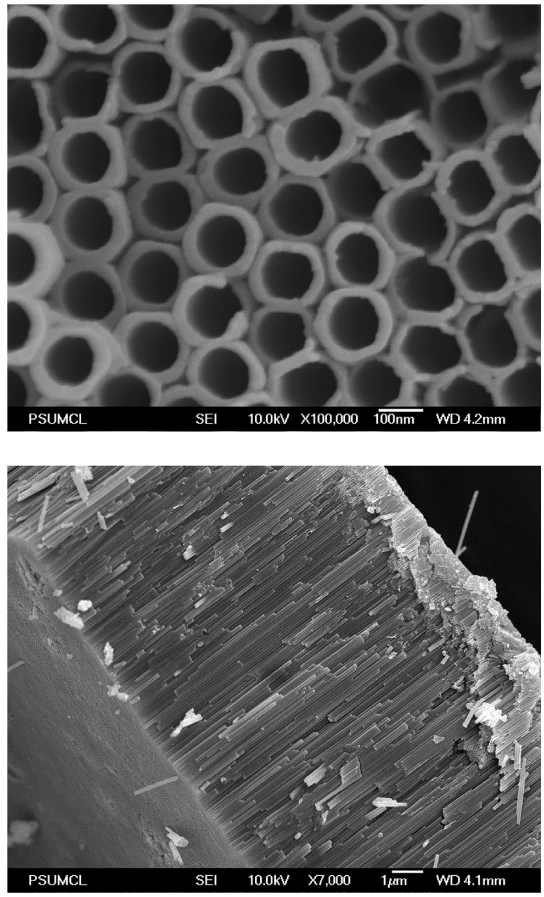

Figure 4. Field emission scanning electron microscope (FESEM) top and cross-sectional images of a mechanically fractured TiO_2 nanotube array sample.

cident light is minimized by the low index of refraction of the nanotube array films.[144]

Nitrogen-doped titania nanotube arrays were synthesized by anodizing titanium foil in an electrolyte consisting of 0.3 M ammonium fluoride (NH_4F) in 2 vol % water containing ethylene glycol at 55 V.[131,145] Samples with nanotube length up to ≈130 μm were prepared by changing the anodization duration. Field emission scanning electron microscope (FESEM) images were used to estimate the average pore diameter and wall thickness of the samples, which were found to about 95 nm (standard deviation 13 nm) and about 20 nm (standard deviation 5 nm), respectively. Nitrogen was incorporated within the nanotubes during the anodization, primarily supplied by the NH_4F and to a lesser extent by the atmospheric nitrogen dissolved into the electrolyte. Anodization of the Ti foil resulted in an amorphous nanotube arrays; hence the nanotube array samples were annealed at 460 or 600 °C for 3 h in oxygen for crystallization. To retain the nitrogen incorporated within the nanotube samples, oxygen flow across the sample during annealing was carefully controlled. Ultrathin layers of copper or platinum were then coated onto the top surface of the nanotube array films using dc sputtering (dc power 1.8 W/cm^2, pressure 20 mTorr, 5 cm distance between target and sample, sputtering time 13 s for Pt and 40 s for Cu). High-resolution transmission electron microscopy (HRTEM) images revealed that nanoscale Pt islands (or copper depending upon sputtering target) were formed on the nanotube walls near the open ends of the tubes (see Figure 5).

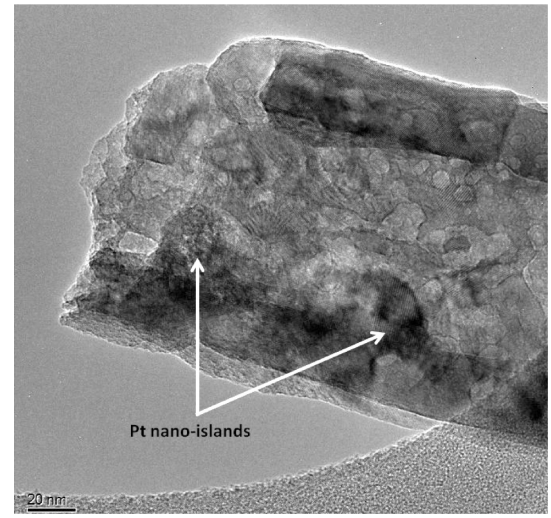

Figure 5. High-resolution transmission electron microscope (HRTEM) image showing nanoscale Pt islands on TiO_2 nanotube walls.

Digital photographs of samples prepared under different conditions are shown in Figure 6. Figure 6a is an as-synthesized 32 μm long nanotube array sample, while Figure 6b,c shows, respectively, 25 and 130 μm long nanotube array samples annealed at 460 °C. The 40 and 130 μm long nanotube arrays annealed at 600 °C are shown in Figure 6d,e, respectively. The absorbance spectra of the 35 and 130 μm samples annealed at 460 °C, and 130 μm sample annealed at 600 °C, are given in Figure 7. For the 460 °C annealed samples, the color changed from dark green to yellowish green as the thickness increased from a few tens of micrometers to 100 μm, while the samples became pale yellow to deep yellow after annealing at 600 °C. The color change with increasing nanotube length is due to the increased absorption of the weakly absorbed wavelengths as the light traverses across a greater path length. X-ray photoelectron spectroscopy (XPS) data were collected from the backside of the nanotube array membranes to avoid errors associated with determining elemental concentrations from a porous surface.[125] The XPS determined nitrogen concentrations were 0.75 atom percent (atom %) for 460 °C annealed samples and 0.4 atom % for 600 °C annealed samples.

Photocatalytic experiments were performed with 2 cm × 2 cm size samples in specially designed reaction chambers (see Figure 8), fitted with gas inlet and outlet valves, a septum attached port for gas sampling, and a quartz window for admitting solar radiation. These reaction chambers were illuminated under outdoor sun-

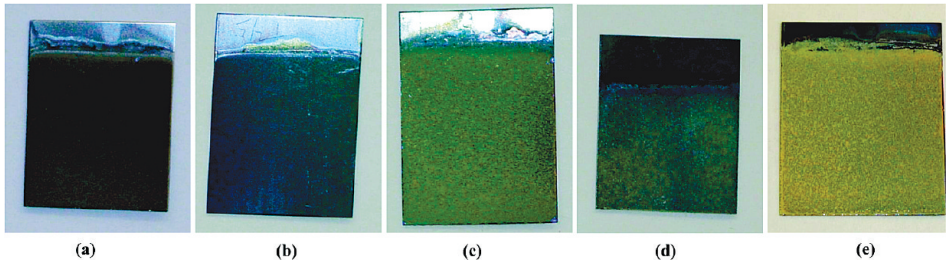

Figure 6. (a) A 32 μm long as-prepared nanotube array sample; (b,c) 25 and 130 μm long nanotube array samples, respectively, annealed at 460 °C; (d,e) 40 and 130 μm long, respectively, nanotube array samples annealed at 600 °C.

light, the intensity (power density) of which was measured at regular intervals using calibrated thermopile detector; the corresponding solar spectra were also recorded using an optical spectrometer (model OSM 2-400DUV-U, Newport Corporation). Since the average power density varied slightly day to day, the product formation rate was normalized to a global AM 1.5 value of 100 mW/cm^2. Data were only recorded when the solar power density varied between about 102 and 75 mW/cm^2. After exposure to sunlight for a noted duration, the residual gas samples were collected from the chambers and analyzed using a Shimadzu (GC-17A) gas chromatograph equipped with flame ionization and thermal conductivity detectors.

Figure 9 shows the hydrocarbon generation rates for 600 °C annealed samples surface-decorated with nanoparticles of Pt (labeled NT/Pt ≈ 35 μm long) or Cu (NT/Cu ≈ 50 μm long). A hydrocarbon production rate of approximately 104 ppm/cm^2 · h (0.78 μL/cm^2 · h or 31.9 nmol/cm^2 · h) was obtained with the 600 °C annealed copper-catalyzed sample. This rate of production obtained under outdoor sunlight (≈150 μL/g · h) was at least 20 times higher than those previously obtained although under laboratory conditions using UV illumination.[101,102,112,113] Experiments done with NT/Pt samples of different nanotube length showed an increase in hydrocarbon production rates up to a nanotube length of about 25 μm; no definite correlation between the reaction rates and nanotube length was obtained for lengths between 25 and 70 μm, and beyond this nanotube length, generally a decrease in production rate was observed. This behavior was attributed to the distribution of catalyst Pt nanoparticles concentrated near the tube openings. It is believed that superior rates of hydrocarbon production would be achieved with a uniform distribution of nanoparticles upon the nanotube surfaces.

As seen in Figure 9, an important difference between the NT/Pt and NT/Cu samples was the amount of H_2 and CO intermediates. With the NT/Pt samples, the H_2 generation rate exceeded the hydrocarbon rate, whereas with the NT/Cu samples, this rate was comparatively low. The NT/Cu samples generated approximately five times more CO than the NT/Pt samples. Considering all products, the total production rate using the NT/Pt samples was about 273 ppm/cm^2 · h.

Since cocatalysts Pt and Cu influence product formation in different ways, with a view toward enhancing hydrocarbon production rates, the two cocatalysts were deposited (by dc sputtering) on different regions of a single 600 °C annealed 40 μm long nanotubes array sample. A nanotube array sample with approximately 52% of the surface area decorated by Cu nanoparticles, and the remaining surface area by Pt nanoparticles, showed an enhanced hydrocarbon generation rate of about 111 ppm/cm^2 · h (≈160 μL/g · h or 0.83 μL/cm^2 · h) with no measurable carbon monoxide generation, as shown in Figure 10a. This result suggested that a homogeneous distribution of cocatalyst nanoparticles over the entire nanotube array surface would significantly improve hydrocarbon generation rates. Therefore, we used a wet chemistry route to deposit copper nanoparticles uniformly on the surface of a 600 °C annealed 50 μm long nitrogen-doped titania nanotube array film. The preliminary results (Figure 10b) show a total hydrocarbon generation rate of about 227

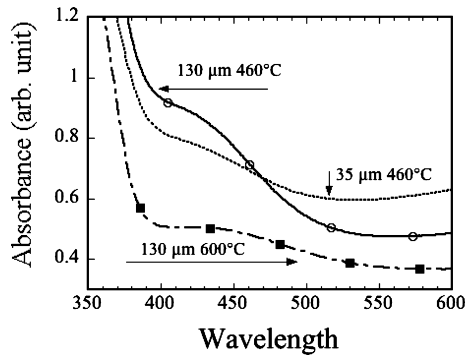

Figure 7. Absorbance spectra of NT array samples of different tube lengths and annealing temperatures.

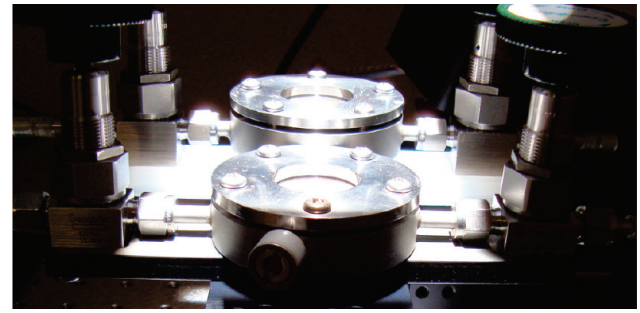

Figure 8. Digital photograph of reaction chambers used for photocatalytic CO_2 reduction experiments kept under simulated sunlight.

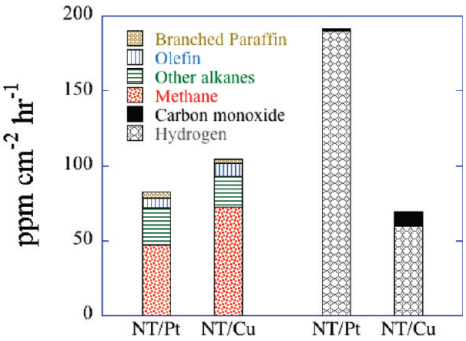

Figure 9. Hydrocarbon, H_2, and CO generation rates for 600 °C annealed nanotube array samples with Cu or Pt catalyst. The Pt-decorated sample is ≈35 μm in length, and the Cu-decorated samples are ≈50 μm in length.

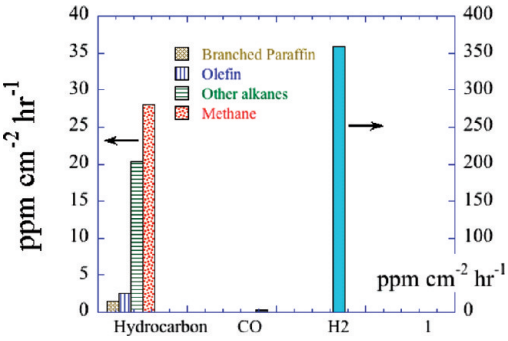

Figure 11. Hydrocarbon, H_2, and CO generation rates of Pd-catalyzed nanotube array sample 35 μm long, 600 °C annealed.

ppm/cm^2 · h (≈280 μL/g · h or 1.7 μL/cm^2 · h) and a total product (hydrocarbons, hydrogen, and carbon monoxide) formation rate of about 783 ppm/cm^2 · h. Work is underway to enhance the conversion rate further with process optimization and a uniform distribution of Pt and Cu nanoparticles on the nanotube surface.

Product selectivity can be tuned by choosing an appropriate cocatalyst material. Figure 11 shows hydrocarbon, carbon monoxide, and hydrogen generation rates from a TiO_2 nanotube array sample 35 μm long and 600 °C annealed cocatalyzed with Pd nanoparticles on the top surface (deposited by dc sputtering). Compared to Cu or Pt cocatalyzed samples, the NT-Pd samples yielded significantly higher rates of hydrogen production.

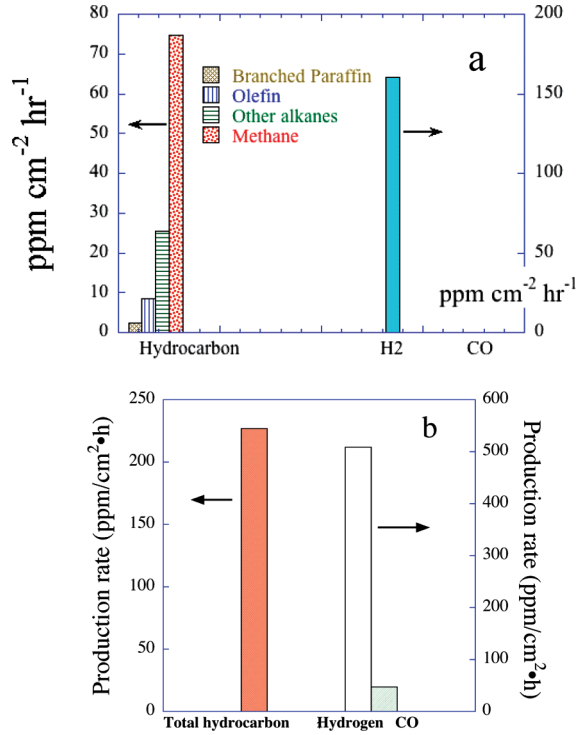

Figure 10. (a) Hydrocarbon and H_2 generation rates from 600 °C annealed nanotube array samples, ≈40 μm in length, surface loaded with both Cu and Pt catalysts using dc sputtering. Nearly 52% of the sample surface area was decorated with Pt nanoparticles, the remaining with Cu nanoparticles. (b) Product rates from a similar sample with nanotube length 50 μm and a uniform distribution of copper nanoparticles deposited using a wet chemistry route over the entire nanotube area.

Figure 12 is illustrative of how variation in a given cocatalyst can alter the final reactant stream. Figure 12a shows, directly from the gas chromatograph, the reactant mixture obtained from photocatalytic reduction of CO_2 + water vapor using nitrogen-doped nanotube arrays with the top surface sensitized with a thin layer of sputter deposited Cu nanoparticles. FESEM studies show the sputtered island-like Cu particles to be planar, with a spatial extent of approximately 20 nm. Figure 12b shows the reactant output with the nanotube arrays sensitized by Cu nanoparticles by dipping in a colloidal solution. We speculate that the difference in the particle size and/or triple phase regions (photocatalyst, cocatalyst, reactant gas interface) created by the colloidal Cu nanoparticles and sputtered Cu islands on the nanotube surface is responsible for the variability in the rate of formation of the various hydrocarbons. However, detailed mechanistic studies are required to obtain in-depth knowledge on the selectivity for methane formation in the case of Cu nanoparticle cocatalysts.

A nanotube array sample (area 3.9 cm^2, 88 mW/cm^2 average sunlight illumination for 3.5 h) without cocatalyst surface loading yielded a nominal hydrocarbon concentration of 10.5 ppm, indicating that without an appropriate cocatalyst titania cannot efficiently drive the CO_2 conversion reaction, a behavior that can be understood by analyzing the relative band-edge positions with respect to the reduction potential of CO_2. A recent study showed the flat band potentials of titania nanotube arrays of lengths 0.5 and 1.0 μm are −0.49 and −0.32 V, respectively, at the isoelectric point of anatase titania (pH = 5.8).[146] These are close to the reduction potential of water, which is −0.34 V (*vs* NHE) at this pH. However, the reduction potential of CO_2 is about 0.11 V more negative than that of water.[104] Therefore, titania cannot effectively reduce CO_2 without having a high electron degeneracy. Temperature-programmed desorption studies conducted on hydrothermally prepared titania nanotubes by Yu and coworkers indicated that the ability of the nanotubes to

adsorb CO_2 was considerably enhanced by Pt nanoparticle loading.[147] In photocatalytic application of Pt nanoparticle loaded titania, it was hypothesized that the photoexcited electrons were trapped by the Pt islands, which then transferred them to surface species for reduction.[148]

We have made preliminary investigations into the effect of multiple sun intensity on the product formation rate using a Class A solar simulator (Newport 91198A, Oriel Instruments, USA) able to provide up to 3.5 sun illumination. TiO_2 nanotube array samples, ≈15 μm in length synthesized using an ethylene glycol electrolyte,[125] were used, cocatalyst sensitized (by dc sputtering) with Cu nanoparticles on half of the sample surface, Pt nanoparticles on the other half. Figure 13a shows the product formation rates of different alkane components as a function of solar intensity. For the same nanotube array sample, a methane formation rate of 30 ppm/cm^2 · h was obtained under 1 sun (nominal sample temperature ≈ 45 °C), with 160 ppm/cm^2 · h found for 3.5 sun illumination (nominal sample temperature 80 °C). Corresponding values for hydrogen, carbon monoxide, and total hydrocarbon (alkane + olefin + branched paraffin) yield are shown in Figure 13b. The total hydrocarbon formation rate shows an increase from 90 ppm/cm^2 · h at 1 sun to about 450 ppm/cm^2 · h under 3.5 sun, a 5-fold increase in the hydrocarbon yield.

Since increased solar intensity is accompanied by an increase in temperature, we investigated the effect of elevated temperature on the product formation rate keeping the sample under 1 sun irradiation. Under 2 sun illumination, the sample temperature is 55 °C. Figure 13c shows the comparative product formation data from a sample illuminated at 1 sun but heated to 55 °C by use of a hot plate, and a sample under 2 sun illumination with a nominal temperature of 55 °C. With constant temperature, the 2 sun illuminated sample saw a 50% increase in the product yield with a doubling of illumination intensity. Our experiments in the dark and in sun, but without a nanotube array sample, did not yield any products within the detection limits of the gas chromatograph. Further experiments are presently underway to understand the effects of temperature and the contributions of thermal (IR) and visible parts of the solar radiation on the photocatalytic processes.

Photocatalytic Processes and Solar Light Conversion Efficiency. It had been earlier shown that CO_2 could be reduced to CO and O_2 using Pt/TiO_2 catalysts.[147] On the basis of this observation, Varghese *et al.*[125] hypothesized that a likely process in the photocatalytic reduction of CO_2 by Cu- or Pt-catalyzed TiO_2 NT samples could be the reaction

$$CO_2 + 2e^- + 2h^+ \rightarrow CO + {}^1/_2O_2 \qquad (11)$$

The oxidation−reduction reaction 8 could occur in several elementary steps, for example, as in 8a−8d:

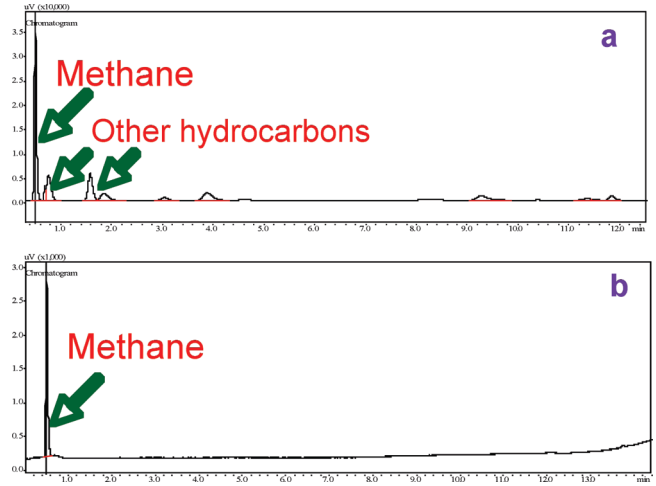

Figure 12. Data illustrating how variation in a given cocatalyst can alter the final reactant stream. (a) Reactant mixture obtained from photocatalytic reduction of CO_2 + water vapor using nanotube arrays with the top surface sensitized with a thin layer of sputter deposited planar Cu having a spatial extent of ≈20 nm. (b) Reactant output with the nanotube arrays sensitized by Cu nanoparticles synthesized and deposited by a wet chemistry route.

$$CO_2 + H^+ + e^- \rightarrow HCO_{2(ads)} \qquad (11a)$$

$$HCO_{2(ads)} + H^+ + e^- \rightarrow CO + H_2O \qquad (11b)$$

$$2H_2O + 2h^+ \rightarrow 2OH_{(ads)} + 2H^+ \qquad (11c)$$

$$2OH_{(ads)} \rightarrow {}^1/_2O_2 + H_2O \qquad (11d)$$

The CO formed in this way would react with atomic hydrogen to form hydrocarbon. On the basis of this, the following mechanism for the conversion of CO_2 into methane was proposed:[125]

$$H_2O + h^+ \rightarrow OH^{\bullet} + H^+ \qquad (12)$$

$$2CO_2 + 4e^- + 4h^+ \rightarrow 2CO + O_2 \qquad (13)$$

$$CO + 6e^- + 6H^+ \rightarrow CH_4 + H_2O \qquad (14)$$

The free energy for overall methane formation

$$CO_2 + 2H_2O(g) \rightarrow CH_4 + 2O_2 \qquad (15)$$

is about 801 kJ/mol, a process requiring 8 photons. The role of the OH radicals and oxygen in the possible back reactions remains unclear.

Water and carbon dioxide splitting processes take place simultaneously on the photocatalyst/cocatalyst surface, and thermodynamic requirements of these processes put constraints on the band gap of the materials used as photocatalysts. Hydrogen formation from water involves a free energy change (ΔG^0) of 237 kJ/mol and an enthalpy change (ΔH^0) of 285 kJ/mol; the corresponding values for CO formation from CO_2 are 257 and 283 kJ/mol at 25 °C (1 atm). Hence, the minimum energy required for water and CO_2 splitting processes are, respectively, 1.229 and 1.33 eV (per photon).

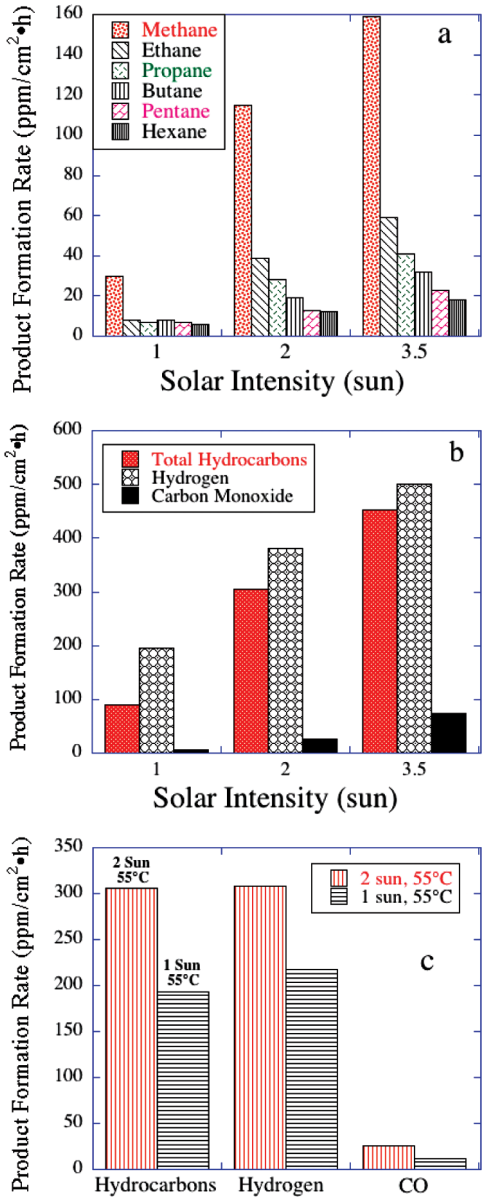

Figure 13. Using TiO_2 nanotube array samples, ≈15 μm in length synthesized using an ethylene glycol electrolyte, co-catalyst sensitized (by dc sputtering) with Cu nanoparticles on half of the sample surface, Pt nanoparticles on the other half: (a) product formation rates of different alkane components as a function of solar intensity. (b) Corresponding values for hydrogen, carbon monoxide, and total hydrocarbon (alkane + olefin + branched paraffin). (c) Comparative product formation rate from a sample illuminated at 1 sun but heated to 55 °C by use of a hot plate, and the same sample under 2 sun illumination with a nominal temperature of ≈55 °C.

In theory, the band gap of a photocatalyst used for co-splitting of CO_2 and water should be at least 1.33 eV, which corresponds to absorption of solar photons of wavelengths below about 930 nm. Considering the energy loss associated with entropy change (about 87 J/mol · K) and other losses involved in the CO_2 splitting process (forming CO and O_2), a band gap between 2 and 2.4 eV is optimal.[149,150] This limits the maximum attainable efficiency to about 17%. However, to date obtained efficiencies are much lower.

For example, consider the case of titania nanotube photocatalysts sensitized with both Pt and Cu nanoparticles that yielded about 111 ppm/cm^2 · h hydrocarbons and 168 ppm/cm^2 · h hydrogen (Figure 10a). The solar conversion (photon to chemical energy) efficiency η can be calculated as η = total energy that can be obtained from the products divided by the incident solar energy. This relation may be given in terms of incident power density (P) and rate of formation (R_i) in mol/s (per unit area) of a component "i" in the products as

$$\eta = (\Sigma_i \mathrm{LHV}_i R_i)/P$$

where LHV is the lower heating value of the component i. Considering the energy output from only paraffins and olefins (up to C6 chains) and hydrogen (energy from olefin and branched paraffins were not taken into account for the sake of simplicity) produced using nanotubes sensitized with Pt and Cu the value of η obtained is ≈0.015%. For nanotube arrays uniformly sensitized with copper nanoparticles η increased to approximately 0.03% (Figure 10b) with a total product generation rate of 783 ppm/cm^2 · h. Contributions from branched paraffins and longer chain hydrocarbons, which we do not consider in the efficiency calculation, should not substantially increase the efficiency value. Although this efficiency is low, it appears to be considerably better than the values other groups obtained using ultraviolet irradiation and is only an order of magnitude lower than what is generally obtained using photosynthesis.[114] Considering the nascent nature of the field, we are optimistic that the conversion efficiency can be increased several orders of magnitude.

It is evident form Figure 7 that the absorbance exhibited by nanotubes for above band gap radiation is excellent. Therefore, the low solar conversion efficiency is not associated with light absorption but more likely with the charge transfer kinetics. The quantum efficiency can be calculated using the relation[97]

$$\mathrm{QE} = (\Sigma_i M_i n_i)/P_m$$

Here M_i is the molar concentration of component i, n_i is number of electrons taking part in the synthesis of component i (for example, $n = 8$ in the case of methane as eight electrons take part in the methane formation reaction), and P_m is molar concentration of incident photons.

For calculating quantum efficiency, a nanotube sample supporting Cu and Pt nanoparticles was exposed to 337 nm radiation (full width half-maximum of the intensity = 10 nm) for 2 h and the product concentrations estimated using a Shimadzu GC2014 gas chromatograph. Concentrations of only paraffins and olefins (up to C6 compounds) were used for calculation. A quantum efficiency of 0.74% was obtained. The quantum efficiency and absorbance data indicate that charge transfer should be enhanced and/or back reac-

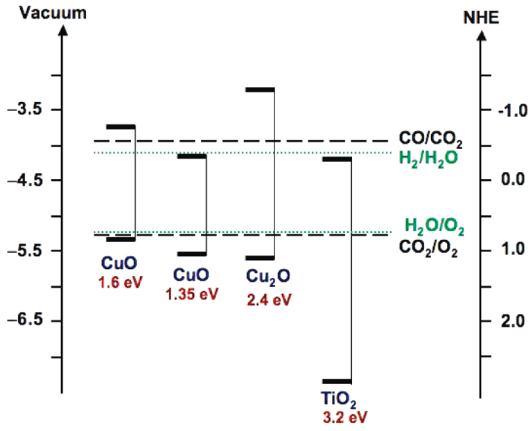

Figure 14. Band-edge positions of CuO, Cu_2O, and anatase TiO_2 in contact with water vapor and CO_2.

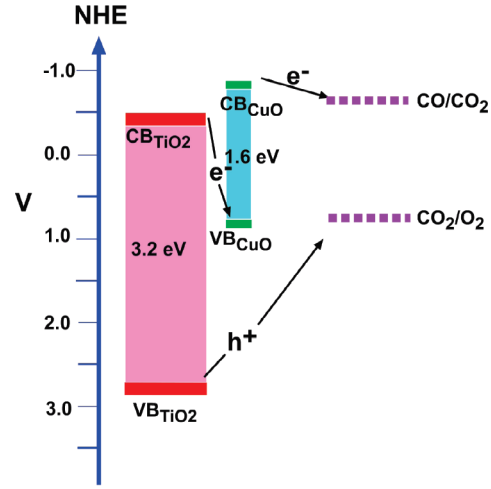

Figure 15. Possible reaction pathways for the photogenerated electron−hole pairs in a TiO_2−CuO system.

tions should be inhibited to achieve high solar to chemical energy conversion efficiencies.

Figure 14 shows the approximate flat band positions of titania as well as the redox potentials for H_2O and CO_2 splitting reactions at pH = 7 with respect to NHE (normal hydrogen electrode) or vacuum. The TiO_2 conduction band is lower than the CO/CO_2 potential. Hence spontaneous transfer of electrons from the titania conduction band to CO_2 occurs only if there is a high electron degeneracy, indicating that a catalyst able to take photogenerated electrons from the titania conduction band is necessary. This has been confirmed by experiments we conducted using titania nanotube arrays without cocatalyst sensitization, which showed no detectable hydrocarbons. Therefore, it is apparent that both platinum and copper help charge carrier transfer between titania and the reactant species.

While metallic cocatalysts are found to be most useful for helping TiO_2 in reduction of CO_2, there exists the possibility of using oxide photcatalysts with appropriate band positions. For example, the CuO band gap varies from 1.3 to 1.7 eV,[151,152] with the flat band potentials varying, as well; two CuO examples are included in Figure 14, 1.35[101] and 1.6 eV[152] band gaps. The valence band energies of CuO and Cu_2O lie near the CO_2/O_2 potential, indicating the likelihood of back reactions. Consequently, the pairing of TiO_2 with either CuO or, ideally, Cu_2O appears appropriate for direct photocatalytic CO_2 conversion. On the basis of the energy band diagram, Figure 15 indicates a possible scheme for the use of photogenerated electron hole pairs in a TiO_2−CuO system for photocatalysis.

With respect to nitrogen doping of the nanotube arrays, it was found that the contribution from wavelengths above 400 nm to photocatalytic hydrocarbon production was about 3% of the total. Lindgren *et al.* observed that only 6 to 7 electrons are produced per 100 photons (internal quantum efficiency 6.8%) within the maximum visible light absorption region (between 400 and 450 nm) in a 850 nm thick nitrogen-doped nanocrystalline porous titania film.[153] It appears that the nitrogen doping creates trap states, such as Ti^{3+} within the TiO_2 band gap,[154,155] that in turn lead to unwanted charge recombination.[156,157]

Before concluding, we would like to make a comment on an article published recently by Wang *et al.*[158] The authors used CdSe quantum dot (QD) loaded on platinum impregnated titania nanoparticles (CdSe/Pt/TiO_2) for visible light activated (>420 nm filtered light from a Xe arc lamp) CO_2 reduction and obtained 48 ppm · g^{-1} · h^{-1} (0.6 μmol · g^{-1} · h^{-1}) methane and traces of methanol, CO, and H_2. While this conversion rate is about 10% of the hydrocarbon generation rate obtained in the case of nitrogen-doped titania nanotubes under direct sunlight,[123] there is a serious issue associated with the process explained in the article. Titania nanoparticles do not absorb the wavelengths (>420 nm) used for the experiment and in that case no photocatalytic activity from TiO_2 could be expected. Although QDs absorb visible light, it cannot oxidize water due to the unfavorable band positioning as shown in Figure 1 of the article (further, this figure is incorrect as pH value and positions of bands do not match). Furthermore, the QDs degraded after 6 h of light exposure. These facts raise doubts as to whether the products observed were really from a visible light photocatalytic process. We suggest that it is necessary to verify the thermodynamic feasibility of a photocatalytic process prior to the use of exotic materials for the purpose.

CONCLUSIONS

Renewable energy sources offer several benefits, including a basis for a sustainable society, a cleaner and healthier environment, and an energy source for which one does not need to export significant amounts of capitol. A key drawback of solar energy is that it is intermittent; hence a means is required for energy storage. The ideal way of storing solar energy is to convert it into a fuel, ideally one that is energy dense, readily transportable, and relatively safe to use. To that end, we con-

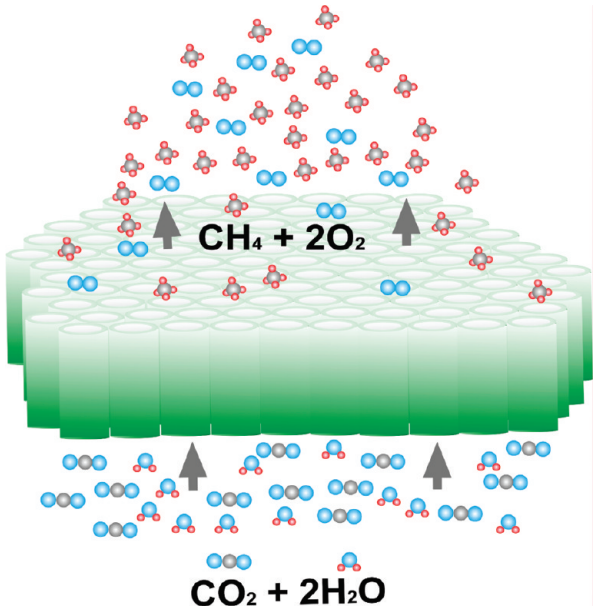

Figure 16. Depiction of flow-through photocatalytic membrane for CO_2 conversion.

sider herein a means for using sunlight to convert CO_2 and water vapor into hydrocarbon fuels that are compatible with the current energy infrastructure. Ideally, such solar energy powered photocatalytic materials, used on a closed-loop basis as depicted in Figure 1, can be used to recycle CO_2 from a climate altering waste product into a fuel.

While encouraging progress has been achieved toward photocatalytic conversion of CO_2 using sunlight, further effort is required for increasing sunlight-to-fuel photoconversion efficiencies. Immediate research opportunities include uniform cocatalyst sensitization of the entire nanotube array surface for enhanced conversion rates, and the design of cocatalysts to improve and control the product selectivity. Highly efficient photocatalytic materials will enable the use of flow-through photocatalytic membranes, wherein CO_2 and water vapor would enter one side of the nanotube array membrane with a fuel exiting from the other (see Figure 16). Paulose *et al.* have reported fabrication of free-standing, mechanically robust, TiO_2 nanotube array membranes of uniform pore size with thicknesses ranging from 4.4 μm to 1 mm;[91] work is currently underway to explore such membranes for photocatalytic reduction of CO_2.

Acknowledgment. Support of this work by the National Science Foundation, CBET-0927262, and the Department of Energy ARPA-E, DE-AR0000008, is gratefully acknowledged. The authors thank Prof. Thomas E. Mallouk of the Pennsylvania State University for helpful comments and suggestions.

REFERENCES AND NOTES

1. Energy Information Administration. *Annual Energy Review*; U.S. Department of Energy, **2008**.
2. Lal, R. Sequestration of Atmospheric CO_2 in Global Carbon Pool. *Energy Environ. Sci.* **2008**, *1*, 86–100.
3. Cohon, J. L. *The Hidden Costs of Energy: Unpriced Consequences of Energy Production and Use*; National Academies Press **2009**, ISBN-10: 0-309-14640-2.
4. Morton, O. *Eating the Sun: How Plants Power the Planet*; Harper: New York, 2008.
5. IPCC Third Assessment Report-Climate Change 2001 (http://www.grida.no/publications/other/ipcc_tar/?src=/climate/ipcc_tar/wg1/339.htm).
6. Hansen, J.; Kharecha, P.; Beerling, D.; Berner, R.; Masson-Delmotte, V.; Pagani, M.; Raymo, M.; Royer, D. L.; Zachos, J. C. Target Atmospheric CO_2: Where Should Humanity Aim? *J. Open Atmos. Sci.* **2008**, *2*, 217–231.
7. Hansen, J. E. Scientific Reticence and Sea Level Rise. *Environ. Res. Lett.* **2007**, *2*, 024002.
8. Schlesinger, W. H.; Reynolds, J. F.; Cunningham, G. L. Biological Feedbacks in Global Desertification. *Science* **1990**, *247*, 1043–1048.
9. Scheffer, M.; Carpenter, S. R. Catastrophic Regime Shifts in Ecosystems: Linking Theory to Observation. *Trends Ecol. Evol.* **2003**, *18*, 648–656.
10. http://fossil.energy.gov/sequestration/geologic/index.html, U.S. Department of Energy.
11. Singh, D.; Croiset, E.; Douglas, P. L.; Douglas, M. A. Techno-Economic Study of CO_2 Capture from an Existing Coal-Fired Power Plant: MEA Scrubbing vs. O_2/CO_2 Recycle Combustion. *Energy Convers. Manage.* **2003**, *44*, 3073–3091.
12. Rao, A.; Rubin, E. A. Technical, Economic, and Environmental Assessment of Amine-Based CO_2 Capture Technology for Power Plant Greenhouse Gas Control. *Environ. Sci. Technol.* **2002**, *36*, 4467–4475.
13. White, C. M.; Strazisar, B. R.; Granite, E. J.; Hoffman, J. S.; Pennline, H. W. Separation and Capture of CO_2 from Large Stationary Sources and Sequestration in Geological Formations—Coal Beds and Deep Saline Aquifers. *J. Air Waste Manage. Assoc.* **2003**, *53*, 645–715.
14. Voormeij, D. A.; Simandl, G. J. Geological, Ocean, and Mineral CO_2 Sequestration Options: A Technical Review. *Geosci. Canada* **2004**, *31*, 11–22.
15. House, K. Z.; Harvey, C. F.; Aziz, M. J.; Schrag, D. P. The Energy Penalty of Post-Combustion CO_2 Capture and Storage and Its Implications for Retrofitting the US Installed Base. *Energy Environ. Sci.* **2009**, *2*, 193–205.
16. Halbwachs, M.; Sabroux, J. C. Removing CO_2 from Lake Nyos in Cameroon. *Science* **2001**, *292*, 438.
17. Chisti, Y. Biodiesel from Microalgae. *Biotechnol. Adv.* **2007**, *25*, 294–306.
18. Sharma, Y. C.; Singh, B.; Upadyay, S. N. Advancements in Development and Characterization of Biodiesel: A Review. *Fuel* **2008**, *87*, 2355–2373.
19. von Blottnitz, H.; Curran, M. A. A Review of Assessments Conducted on Bio-ethanol as a Transportation Fuel from a Net Energy, Greenhouse Gas, and Environmental Life Cycle Perspective. *J. Cleaner Prod.* **2007**, *15*, 607–619.
20. Ma, F.; Hanna, M. A. Biodiesel Production: A Review. *Biores. Technol.* **1999**, *70*, 1–15.
21. Chisti, Y. Biodiesel from Microalgae Beats Bioethanol. *Trends Biotechnol.* **2008**, *28*, 126–131.
22. Sauerbeck, D. R. CO_2 Emissions and C Sequestration by Agriculture—Perspectives and Limitations. *Nutr. Cycl. Agroecosyst.* **2001**, *60*, 153–266.
23. Gao, K.; McKinley, K. R. Use of Macroalgae for Marine Biomass Production and CO_2 Remediation: A Review. *J. Appl. Phycology* **1994**, *6*, 45–70.
24. Zelitch, I. Improving the Efficiency of Photosynthesis. *Science* **1975**, *188*, 626–633. Lewis, N. S. Powering the Planet. *MRS Bull.* **2007**, *32*, 808–820.
25. Giampietro, M.; Ulgiati, S.; Pimentel, D. Feasibility of Large-Scale Biofuel Production. *BioScience* **1997**, *47*, 587–600.
26. Olah, G. A.; Goeppert, A.; Prakash, G. K. S. Chemical Recycling of Carbon Dioxide to Methanol and Dimethyl Ether: From Greenhouse Gas to Renewable, Environmentally Carbon Neutral Fuels and Synthetic Hydrocarbons. *J. Org. Chem.* **2009**, *74*, 487–498.

27. Gattrell, M.; Gupta, N.; Co, A. Electrochemical Reduction of CO_2 to Hydrocarbons to Store Renewable Electrical Energy and Upgrade Biogas. *Energy Convers. Manage.* **2007**, *48*, 1255–1265.
28. Halmann, M. M.; Steinberg, M. *Greenhouse Gas Carbon Dioxide Mitigation: Science and Technology*, 1st ed.; CRC Press: New York, 1998.
29. Gilkeson, M. M.; White, R. R.; Sliepcevich, C. M. Synthesis of Methane—By Hydrogenation of Carbon Monoxide in a Tubular Reactor. *Ind. Eng. Chem.* **1953**, *45*, 460–467.
30. Song, C. Global Challenges and Strategies for Control, Conversion and Utilization of CO_2 for Sustainable Development Involving Energy, Catalysis, Adsorption and Chemical Processing. *Catal. Today* **2006**, *115*, 2–32.
31. Hashimoto, K.; Habazaki, H.; Yamasaki, M.; Meguro, S.; Sakaki, T.; Katagiri, H.; Matsui, T.; Fujimara, K.; Izumiya, K.; Kumagai, H.; Akiyama, E. Advanced Materials for Global Carbon Dioxide Recycling. *Mater. Sci. Eng., A* **2001**, *304*−*306*, 88–96.
32. Martin, L. R. Use of Solar Energy to Reduce Carbon Dioxide. *Sol. Energy* **1980**, *24*, 271–277.
33. Galvez, M. E.; Loutzenhiser, P. G.; Hischier, I.; Steinfeld, A. CO_2 Splitting *via* Two-Step Solar Thermochemical Cycles with Zn/ZnO and FeO/Fe_3O_4 Redox Reactions: Thermodynamic Analysis. *Energy Fuel* **2008**, *22*, 3544–3550.
34. Traynor, A. J.; Jensen, R. J. Direct Solar Reduction of CO_2 to Fuel: First Prototype Results. *Ind. Eng. Chem. Res.* **2002**, *41*, 1935–1939.
35. Grimes, C. A.; Varghese, O. K.; Ranjan, S. *Light, Water, Hydrogen: The Solar Generation of Hydrogen by Water Photoelectrolysis*; Springer: New York, 2007.
36. Dorner, S.; Keller, C. Hydrogen Production from Decomposition of Water by Means of Nuclear Reactor Heat, Hydrogen Energy. Proceedings of the Hydrogen Economy Miami Energy Conference, 1974; pp 155−166.
37. Bamberger, C. E.; Robinson, P. R. Thermochemical Splitting of Water and Carbon Dioxide with Cerium Compounds. *Inorg. Chim. Acta* **1980**, *42*, 133–137.
38. Diver, R. B.; Miller, J. E.; Allendorf, M. D.; Siegel, N. P.; Hogan, R. E. Solar Thermochemical Water Splitting Ferrite-Cycle Heat Engines. *J. Sol. Energy Eng.* **2008**, *130*, 041001-1–041001-8.
39. Centi, G.; Perathoner, S.; Rak, Z. S. Reduction of Greenhouse Gas Emissions by Catalytic Processes. *Appl. Catal. B: Environ.* **2003**, *41*, 143–155.
40. Jitaru, M. Electrochemical Carbon Dioxide Reduction—Fundamental and Applied Topics. *J. Univ. Chem. Tech. Metall.* **2007**, *42*, 333–344.
41. Kaneco, S.; Hiei, N.-H.; Katsumata, H.; Ohnishi, H.; Suzuki, T.; Ohta, K. Electrochemical Reduction of Carbon Dioxide to Methane in Aqueous $NaHCO_3$ Solution at Less than 273 K. *Electrochim. Acta* **2002**, *4*, 51–55.
42. Teeter, T. E.; Van Rysselberghe, P. Reduction of Carbon Dioxide on Mercury Cathodes. *J. Chem. Phys.* **1954**, *22*, 759–160.
43. Gattrell, M.; Gupta, N.; Co, A. A Review of the Aqueous Electrochemical Reduction of CO_2 to Hydrocarbons at Copper. *J. Electroanal. Chem.* **2006**, *594*, 1–19.
44. Momose, Y.; Sato, K.; Ohno, O. Electrochemical Reduction of CO_2 at Copper Electrodes and Its Relationship to the Metal Surface Characteristics. *Surf. Interface Anal.* **2002**, *34*, 615–618.
45. Shibata, H.; Moulijn, J. A.; Mul, G. Enabling Electrocatalytic Fischer−Tropsch Synthesis from Carbon Dioxide Over Copper-Based Electrodes. *Catal. Lett.* **2008**, *123*, 186–192.
46. Hori, Y.; Murata, A.; Takahashi, R.; Suzuki, S. Enhanced Formation of Ethylene and Alcohols at Ambient Temperature and Pressure in Electrochemical Reduction of Carbon Dioxide at a Copper Electrode. *J. Chem. Soc., Chem. Commun.* **1988**, 17–19.
47. Noda, H.; Ikeda, S.; Oda, Y.; Imai, K.; Maeda, M.; Ito, K. Electrochemical Reduction of Carbon Dioxide at Various Metal Electrodes in Aqueous Potassium Hydrogen Carbonate Solution. *Bull. Chem. Soc. Jpn.* **1990**, *63*, 2459–2462.
48. Centi, G.; Perathoner, S. Catalysis: Role and Challenges for a Sustainable Energy. *Top. Catal.* **2009**, *52*, 948–961.
49. Jitaru, M.; Lowy, D. A.; Toma, M.; Toma, B. C.; Oniciu, L. Electrochemical Reduction of Carbon Dioxide on Flat Metallic Cathodes. *J. Appl. Electrochem.* **1997**, *27*, 875–889.
50. Sánchez-Sánchez, C. M.; Montiel, V.; Tryk, D. A.; Aldaz, A.; Fujishima, A. Electrochemical Approaches to Alleviation of the Problem of Carbon Dioxide Accumulation. *Pure Appl. Chem.* **2001**, *73*, 1917–1927.
51. Hori, Y.; Kikuchi, K.; Suzuki, S. Production of CO and CH_4 in Electrochemical Reduction of CO_2 at Metal Electrodes in Aqueous Hydrogen Carbonate Solution. *Chem. Lett.* **1985**, 1695–1698.
52. Noda, H.; Ikeda, S.; Yamamoto, A.; Einaga, H.; Ito, K. Kinetics of Electrochemical Reduction of Carbon Dioxide on a Gold Electrode in Phosphate Buffer Solutions. *Bull. Chem. Soc. Jpn.* **1995**, *68*, 1889–1895.
53. Hori, Y.; Murata, A.; Takahashi, R. Formation of Hydrocarbons in the Electrochemical Reduction of Carbon Dioxide at a Copper Electrode in Aqueous Solution. *J. Chem. Soc., Faraday Trans. 1* **1989**, *85*, 2309–2326.
54. Hori, Y.; Konishi, H.; Futamura, T.; Murata, A.; Koga, O.; Sakurai, H.; Oguma, K. 'Deactivation of Copper Electrode' in Electrochemical Reduction of CO_2. *Electrochim. Acta* **2005**, *50*, 5354–5369.
55. Pettinicchi, S.; Boggetti, H.; Lopez de Mishima, B. A.; Mishima, H. T.; Rodriguez, J.; Pastor, E. Electrochemical Reduction of Carbon Dioxide on Copper Alloy. *J. Arg. Chem. Soc.* **2003**, *91*, 107–118.
56. Kudo, K.; Komatsu, K. Selective Formation of Methane in Reduction of CO_2 with Water by Raney Alloy Catalyst. *J. Mol. Catal., A* **1999**, *145*, 257–264.
57. Lukaszewski, M.; Grden, M.; Czerwinski, A. Influence of Adsorbed Carbon Dioxide on Hydrogen Electrosorption in Palladium−Platinum−Rhodium Alloys. *Electrochim. Acta* **2004**, *49*, 3161–3167.
58. Furuya, N.; Yamazaki, T.; Shibata, M. High Performance Ru−Pd Catalysts for CO_2 Reduction at Gas-Diffusion Electrodes. *J. Electroanal. Chem.* **1997**, *431*, 39–41.
59. Koleli, F. K.; Ropke, T. R.; Hamann, C. H. Electrochemical Impedance Spectroscopic Investigation of CO_2 Reduction on Polyaniline in Methanol. *Electrochem. Acta* **2003**, *48*, 1595–1601.
60. Centi, G.; Perathoner, S.; Wine, G.; Gangeri, M. Electrocatalytic Conversion of CO_2 to Long Carbon-Chain Hydrocarbons. *Green Chem.* **2007**, *9*, 671–678.
61. Hori, Y.; Kikuchi, K.; Murata, A.; Suzuki, S. Production of Methane and Ethylene in Electrochemical Reduction of Carbon Dioxide at Copper Electrode in Aqueous Hydrogencarbonate Solution. *Chem. Lett.* **1986**, 897–898.
62. Noda, H.; Ikeda, S.; Oda, Y.; Ito, K. Potential Dependencies of the Products on Electrochemical Reduction of Carbon Dioxide at a Copper Electrode. *Chem. Lett.* **1989**, 289–292.
63. Salimon, J.; Kalaji, M. Electrochemical Reduction of CO_2 at Polycrystalline Copper in Aqueous Phosphate Buffered Solution: pH and Temperature Dependence. *Malaysian J. Chem.* **2003**, *5*, 23–29.
64. Saeki, T.; Hashimoto, K.; Kimura, N.; Omata, K.; Fujishima, A. Electrochemical Reduction of CO_2 with High Current Density in a CO_2 + Methanol Medium at Various Metal Electrodes. *J. Electroanal. Chem.* **1996**, *404*, 299–302.
65. Ohta, K.; Suda, K.; Kaneco, S.; Mizuno, T. Electrochemical Reduction of Carbon Dioxide at Cu Electrode Under Ultrasonic Irradiation. *J. Electrochem. Soc.* **2000**, *147*, 233–237.
66. Hara, K.; Sakata, T. Large Current Density CO_2 Reduction under High Pressure Using Gas Diffusion Electrodes. *Bull. Chem. Soc. Jpn.* **1997**, *70*, 571–576.
67. Tomita, Y.; Teruya, S.; Koga, O.; Hori, Y. Electrochemical Reduction of Carbon Dioxide at a Platinum Electrode in Acetonitrile−Water Mixtures. *J. Electrochem. Soc.* **2000**, *11*, 4164–4167.

68. Kaneco, S.; Iiba, K.; Ohta, K.; Mizuno, T. Electrochemical Reduction of Carbon Dioxide in Methanol with Various Potassium Supporting Electrolytes at Low Temperature. *J. Solid State Electrochem.* **1999**, *3*, 424–428.
69. Kaneco, S.; Iwao, R.; Iiba, K.; Itoh, S.-I.; Ohta, K.; Mizuno, T. Electrochemical Reduction of Carbon Dioxide on an Indium Wire in a KOH/Methanol-Based Electrolyte at Ambient Temperature and Pressure. *Environ. Eng. Sci.* **1999**, *16*, 131–137.
70. Kaneco, S.; Iiba, K.; Hiei, N.-H.; Ohta, K.; Mizuno, T.; Suzuki, T. Electrochemical Reduction of Carbon Dioxide to Ethylene with Faradaic Efficiency at a Cu Electrode in CsOH/Methanol. *Electrochim. Acta* **1999**, *44*, 4701–4706.
71. Mizuno, T.; Naitoh, A.; Ohta, K. Electrochemical Reduction of CO_2 in Methanol at −30 °C. *J. Electroanal. Chem.* **1995**, *391*, 199–201.
72. Saeki, T.; Hashimoto, K.; Fijishima, A.; Kimura, N.; Omata, K. Electrochemical Reduction of CO_2 with High Current Density in a CO_2−Methanol Medium. *J. Phys. Chem.* **1995**, *99*, 8440–8446.
73. Meshitsuka, S.; Ichikawa, M.; Tamaru, K. Electrocatalysis by Metal Phthalocyanines in Reduction of Carbon-Dioxide. *J. Chem. Soc., Chem. Commun.* **1974**, 158–159.
74. Lieber, C. M.; Lewis, N. S. Catalytic Reduction of CO_2 at Carbon Electrodes Modified with Cobalt Phthalocyanine. *J. Am. Chem. Soc.* **1984**, *106*, 5033–5034.
75. Hawecker, J.; Lehn, J. M.; Ziessel, R. Electrocatalytic Reduction of Carbon-Dioxide Mediated by $Re(bipy)(CO)_3Cl$(bipy=2,2′-bipyridine). *J. Chem. Soc., Chem. Commun.* **1984**, 328–330.
76. Slater, S.; Wagenknecht, J. H. Electrochemical Reduction of CO_2 Catalyzed by $Rh(diphos)_2Cl$. *J. Am. Chem. Soc.* **1984**, *106*, 5367–5368.
77. Ogura, K.; Endo, N. Electrochemical Reduction of CO_2 with a Functional Gas-Diffusion Electrode in Aqueous Solutions with and without Propylene Carbonate. *J. Electrochem. Soc.* **1999**, *146*, 3736–3740.
78. Chiericato, G., Jr.; Arana, C. R.; Cadado, C.; Cuadrado, I.; Abruna, H. D. Electrocatalytic Reduction of Carbon dioxide by Transition Metal Complexes with Terdentate Ligands Derived from Diacetylpyridine. *Inorg. Chim. Acta* **2000**, *300−302*, 32–42.
79. Fisher, B.; Eisenberg, R. Electrocatalytic Reduction of Carbon Dioxide by Using Macrocycles of Nickel and Cobalt. *J. Am. Chem. Soc.* **1980**, *102*, 7361.
80. Bhugun, I.; Lexa, D.; Saveant, J. M. Homogeneous Catalysis of Electrochemical Hydrogen Evolution by Iron(0) Porphyrins. *J. Am. Chem. Soc.* **1996**, *118*, 176–184.
81. Delaet, D. L.; Delrosario, R.; Fanwick, P. E.; Kubiak, C. P. Carbon-Dioxide Chemistry and Electrochemistry of a Binuclear Cradle Complex of Ni(0), $Ni_2(\mu$-CNMe$)(CNMe)_2(PPh_2CH_2PPh_2)_2$. *J. Am. Chem. Soc.* **1987**, *109*, 754–758.
82. Simon-Manso, E.; Kubiak, C. P. Dinuclear Nickel Complexes as Catalysts for Electrochemical Reduction of Carbon Dioxide. *Organometallics* **2005**, *24*, 96–102.
83. Benson, E. E.; Kubiak, C. P.; Sathrum, A. J.; Smieja, J. M. Electrocatalytic and Homogeneous Approaches to Conversion of CO_2 to Liquid Fuels. *Chem. Soc. Rev.* **2009**, *38*, 89–99.
84. Zhang, A.; Zhang, W.; Lu, J.; Wallace, G. G.; Chen, J. Electrocatalytic Reduction of Carbon Dioxide by Cobalt−Phthalocyanine Incorporated Polypyrrole. *Electrochem. Solid State Lett.* **2009**, *12*, E17–E19.
85. Gangeri, M.; Perathoner, S.; Caudo, S.; Centi, G.; Amadou, J.; Begin, D.; Pham-Huu, C.; Ledoux, M. J.; Tessonnier, J. -P.; Su, D. S.; Schlogl, R. Fe and Pt Carbon Nanotubes for the Electrocatalytic Conversion of Carbon Dioxide to Oxygenates. *Catal. Today* **2009**, *143*, 57–63.
86. Angamuthu, R.; Byers, P.; Lutz, M.; Spek, A. L.; Bouwmann, E. Electrocatalytic CO_2 Conversion to Oxalate by a Copper Complex. *Science* **2010**, *327*, 313–327.
87. Hara, K.; Kudo, A.; Sakata, T. Electrochemical Reduction of Carbon Dioxide under High Presure on Various Electrodes in an Aqueous Electrolyte. *J. Electroanal. Chem.* **1995**, *391*, 141–147.
88. Bidrawn, F.; Kim, G.; Corre, G.; Irvine, J. T. S.; Vohs, J. M.; Gorte, R. J. Efficient Reduction of CO_2 in a Solid Oxide Electrolyzer. *Electrochem. Solid State* **2008**, *11*, B167–B170.
89. Zhan, Z.; Kobsiriphat, W.; Wilson, J. R.; Pillai, M.; Kim, I.; Barnett, S. A. Syngas Production by Coelectrolysis of CO_2/H_2O: The Basis for a Renewable Energy Cycle. *Energy Fuel* **2009**, *23*, 3089–309.
90. Stoots, C. M.; O'Brien, J. E.; Herring, J. S.; Condie, K. G.; Hartvigsen, J. J. Idaho National Laboratory Experimental Research in High Temperature Electrolysis For Hydrogen and Syngas Production. Proceedings of the 4th International Topical Meeting on High Temperature Reactor Technology, Washington, DC, 2008.
91. Halmann, M. Photoelectrochemical Reduction of Aqueous Carbon-Dioxide on p-Type Gallium-Phosphide in Liquid Junction Solar-Cells. *Nature* **1978**, *275*, 115–116.
92. Canfield, D.; Frese, K. W. Reduction of Carbon-Dioxide to Methanol on n-GaAs and p-GaAs and p-InP: Effect of Crystal-Face, Electrolyte and Current-Density. *J. Electrochem. Soc.* **1983**, *130*, 1772–1773.
93. Blajeni, B. A.; Halmann, M.; Manassen, J. Electrochemical Measurements on the Photo-Electrochemical Reduction of Aqueous Carbon-Dioxide on p-Gallium Phosphide and p-Gallium Arsenide Semiconductor Electrodes. *Sol. Energy Mater.* **1983**, *8*, 425–440.
94. Eggins, B. R.; Irvine, J. T. R.; Murphy, E. P.; Grimshaw, J. Formation of 2-Carbon Acids from Carbon-Dioxide by Photoreduction on Cadmium-Sulfide. *J. Chem. Soc., Chem. Commun.* **1988**, 1123–1124.
95. Fujiwara, H.; Hosokawa, H.; Murakoshi, K.; Wada, Y.; Yanagida, S. Surface Characteristics of ZnS Nanocrystallites Relating to Their Photocatalysis for CO_2 Reduction. *Langmuir* **1998**, *14*, 5154–5159.
96. Kuwabata, S.; Nishida, K.; Tsuda, R.; Inoue, H.; Yoneyama, H. Photochemical Reduction of Carbon Dioxide to Methanol Using ZnS Microcrystallite as a Photocatalyst in the Presence of Methanol Dehydrogenase. *J. Electrochem. Soc.* **1994**, *141*, 1498–1503.
97. Barton, E. E.; Rampulla, D. M.; Bocarsly, A. B. Selective Solar-Driven Reduction of CO_2 to Methanol Using a Catalyzed p-GaP Based Photoelectrochemical Cell. *J. Am. Chem. Soc.* **2008**, *130*, 6342–6344.
98. Inoue, T.; Fujishima, A.; Konishi, S.; Honda, K. Photoelectrocatalytic Reduction of Carbon-Dioxide in Aqueous Suspensions of Semiconductor Powders. *Nature* **1979**, *277*, 637–638.
99. Halmann, M.; Ulman, M.; Blajeni, B. A. Photochemical Solar Collector for the Photoassisted Reduction of Aqueous Carbon-Dioxide. *Sol. Energy* **1983**, *31*, 429–431.
100. Cook, R. L.; Macduff, R. C.; Sammells, A. F. Photoelectrochemical Carbon-Dioxide Reduction to Hydrocarbons at Ambient-Temperature and Pressure. *J. Electrochem. Soc.* **1988**, *135*, 3069–3070.
101. Adachi, K.; Ohta, K.; Mijuma, T. Photocatalytic Reduction of Carbon-Dioxide to Hydrocarbon Using Copper-Loaded Titanium-Dioxide. *Sol. Energy* **1994**, *53*, 187–190.
102. Anpo, M.; Chiba, K. Photocatalytic Reduction of CO_2 on Anchored Titanium-Oxide Catalysts. *J. Mol. Catal.* **1992**, *74*, 207–212.
103. Anpo, M.; Yamashita, H.; Ichihashi, Y.; Fujii, Y.; Honda, M. Photocatalytic Reduction of CO_2 with H_2O on Titanium Oxides Anchored within Micropores of Zeolites: Effects of the Structure of the Active Sites and the Addition of Pt. *J. Phys. Chem. B* **1997**, *101*, 2632–2636.
104. Sayama, K.; Arakawa, H. Photocatalytic Decomposition of Water and Photocatalytic Reduction of Carbon-Dioxide over ZrO_2 Catalyst. *J. Phys. Chem.* **1993**, *97*, 531–533.
105. Ikeue, K.; Nozaki, S.; Ogawa, M.; Anpo, M. Photocatalytic Reduction of CO_2 with H_2O on Ti Containing Porous Silica Thin Film Photocatalyst. *Catal. Lett.* **2002**, *80*, 111–114.
106. Matsumoto, Y.; Obata, M.; Hombo, J. Photocatalytic Reduction of Carbon-Dioxide on p-Type $CaFe_2O_4$ Powder. *J. Phys. Chem.* **1994**, *98*, 2950–2951.
107. Ichikawa, S.; Doi, R. Hydrogen Production from Water and Conversion of Carbon Dioxide to Useful Chemicals by

Room Temperature Photoelectrocatalysis. *Catal. Today* **1996**, *27*, 271–277.
108. Guan, G.; Kida, T.; Yoshida, A. Reduction of Carbon Dioxide with Water under Concentrated Sunlight Using Photocatalyst Combined with Fe-Based Catalyst. *Appl. Catal., B* **2003**, *41*, 387–396.
109. Sasirekha, N.; Basha, S. J. S.; Shanthi, K. Photocatalytic Performance of Ru Doped Anatase Mounted on Silica for Reduction of Carbon Dioxide. *Appl. Catal., B* **2006**, *62*, 169–180.
110. Ulagappan, N.; Frei, H. Mechanistic Study of CO_2 Photoreduction in Ti Silicalite Molecular Sieve by FT-IR spectroscopy. *J. Phys. Chem. A* **2000**, *104*, 7834–7839.
111. Lin, W. Y.; Han, H. X.; Frei, H. CO_2 Splitting by H_2O to CO and O_2 under UV Light in TiMCM-41 Silicate Sieve. *J. Phys. Chem. B* **2004**, *108*, 18269–18273.
112. Tan, S. S.; Zou, L.; Hu, E. Photosynthesis of Hydrogen and Methane as Key Components for Clean Energy System. *Sci. Technol. Adv. Mater.* **2007**, *9*, 89–92.
113. Lo, C. C.; Hung, C. H.; Yuan, C. S.; Wu, J. F. Photoreduction of Carbon Dioxide with H_2 and H_2O over TiO_2 and ZrO_2 in a Circulated Photocatalytic Reactor. *Sol. Energy Mater. Sol. Cells* **2007**, *91*, 1765–1774.
114. Nishimura, A.; Sugiura, N.; Kato, S.; Maruyama, N. *Proc. Int. Energy Convers. Eng. Conf.* Rhode Island, 2004; pp 824−827.
115. Xia, X-H,; Jia, Z.-J.; Yu, Y.; Liang, Y.; Wang, Z.; Ma, L.-L. Preparation of Multi-Walled Carbon Nanotube Supported TiO_2 and Its Photocatalytic Activity in the Reduction of CO_2 with H_2O. *Carbon* **2007**, *45*, 717–721.
116. Wu, J. C. S.; Wu, T.-H.; Chu, T.; Huang, H.; Tsai, D. Application of Optical-Fiber Photoreactor for CO_2 Photocatalytic Reduction. *Top. Catal.* **2008**, *47*, 131–136.
117. Thampi, K. R.; Kiwi, J.; Graetzel, M. Methanation and Photo-Methanation of Carbon-Dioxide at Room-Temperature and Atmospheric-Pressure. *Nature* **1987**, *327*, 506–508.
118. Melsheimer, J.; Guo, W.; Ziegler, D.; Wesemann, M.; Schlogl, R. Methanation of Carbon-Dioxide over Ru Titania at Room-Temperature—Explorations for a Photoassisted Catalytic Reaction. *Catal. Lett.* **1991**, *11*, 157–168.
119. Takeda, H.; Koike, K.; Inoue, H.; Ishitani, O. Development of an Efficient Photocatalytic System for CO_2 Reduction Using Rhenium(I) Complexes Based on Mechanistic Studies. *J. Am. Chem. Soc.* **2008**, *130*, 2023–2031.
120. Lehn, J.-M.; Ziessel, R. Photochemical Generation of Carbon-Monoxide and Hydrogen by Reduction of Carbon-Dioxide and Water under Visible-Light Irradiation. *Proc. Natl. Acad. Sci. U.S.A.* **1982**, *79*, 701–704.
121. Craig, C. A.; Spreer, L. O.; Otvos, J. W.; Calvin, M. Photochemical Reduction of Carbon-Dioxide Using Nickel Tetraazamacrocycles. *J. Phys. Chem.* **1990**, *94*, 7957–7960.
122. Fujita, E. Photochemical Carbon Dioxide Reduction with Metal Complexes. *Coord. Chem. Rev.* **1999**, *185−186*, 373–384.
123. Gholamkhass, B.; Mametsuka, H.; Koike, K.; Tanabe, T.; Furue, M.; Ishitani, O. Architecture of Supramolecular Metal Complexes for Photocatalytic CO_2 Reduction: Ruthenium−Rhenium Bi- and Tetra-Nuclear Complexes. *Inorg. Chem.* **2005**, *44*, 2326–2336.
124. Ozcan, O.; Yukruk, F.; Akkaya, E. U.; Uner, D. Dye Sensitized CO_2 Reduction over Pure and Platinized TiO_2. *Top. Catal.* **2007**, *44*, 523–528.
125. Varghese, O. K.; Paulose, M.; LaTempa, T. J.; Grimes, C. A. High-Rate Solar Photocatalytic Conversion of CO_2 and Water Vapor to Hydrocarbon Fuels. *Nano Lett.* **2009**, *9*, 731–737.
126. Varghese, O. K.; Yang, X.; Kendig, J.; Paulose, M.; Zeng, K.; Palmer, C.; Ong, K. G.; Grimes, C. A. A Transcutaneous Hydrogen Sensor: From Design to Application. *Sens. Lett.* **2006**, *4*, 120–128.
127. Varghese, O. K.; Gong, D.; Paulose, M.; Ong, K. G.; Grimes, C. A. Hydrogen Sensing using Titania Nanotubes. *Sens. Actuators, B* **2003**, *93*, 338–344.
128. Varghese, O. K.; Mor, G. K.; Grimes, C. A.; Paulose, M.; Mukherjee, N. A Titania Nanotube-Array Room-Temperature Sensor for Selective Detection of Hydrogen at Low Concentrations. *J. Nanosci. Nanotechnol.* **2004**, *4*, 733–737.
129. Mor, G. K.; Shankar, K.; Paulose, M.; Varghese, O. K.; Grimes, C. A. Enhanced Photocleavage of Water Using Titania Nanotube Arrays. *Nano Lett.* **2005**, *5*, 191–195.
130. Varghese, O. K.; Paulose, M.; Shankar, K.; Mor, G. K.; Grimes, C. A. Water-Photolysis Properties of Micron-Length Highly-Ordered Titania Nanotube-Arrays. *J. Nanosci. Nanotechnol.* **2005**, *5*, 1158–1165.
131. Paulose, M.; Shankar, K.; Yoriya, S.; Prakasham, H. E.; Varghese, O. K.; Mor, G. K.; LaTempa, T. A.; Fitzerald, A.; Grimes, C. A. Anodic Growth of Highly Ordered TiO_2 Nanotube Arrays to 134 μm in Length. *J. Phys. Chem. B* **2006**, *110*, 16179–16184.
132. Mor, G. K.; Shankar, K.; Paulose, M.; Varghese, O. K.; Grimes, C. A. Use of Highly-Ordered TiO_2 Nanotube Arrays in Dye-Sensitized Solar Cells. *Nano Lett.* **2006**, *6*, 215–218.
133. Paulose, M.; Shankar, K.; Varghese, O. K.; Mor, G. K.; Hardin, B.; Grimes, C. A. Backside Illuminated Dye-Sensitized Solar Cells Based on Titania Nanotube Array Electrodes. *Nanotechnology* **2006**, *17*, 1446–1448.
134. Shankar, K.; Bandara, J.; Paulose, M.; Wietasch, H.; Varghese, O. K.; Mor, G. K.; LaTempa, T. J.; Thelakkat, M.; Grimes, C. A. Highly Efficient Solar Cells Using TiO_2 Nanotube Arrays Sensitized with a Donor-Antenna Dye. *Nano Lett.* **2008**, *8*, 1654–1659.
135. Mor, G. K.; Shankar, K.; Paulose, M.; Varghese, O. K.; Grimes, C. A. High Efficiency Double Heterojunction Polymer Photovoltaic Cells using Highly Ordered TiO_2 Nanotube Arrays. *Appl. Phys. Lett.* **2007**, *91*, 152111.
136. Shankar, K.; Mor, G. K.; Prakasam, H. E.; Yoriya, S.; Paulose, M.; Varghese, O. K.; Grimes, C. A. Highly-Ordered TiO_2 Nanotube-Arrays up to 220 μm in Length: Use in Water Photoelectrolysis and Dye-Sensitized Solar Cells. *Nanotechnol.* **2007**, *18*, 065707.
137. Peng, L.; Mendelsohn, A. D.; LaTempa, T. J.; Yoriya, S.; Grimes, C. A.; Desai, T. A. Long-Term Small Molecule and Protein Elution from TiO_2 Nanotubes. *Nano Lett.* **2009**, *9*, 1932–1936.
138. Peng, L.; Eltgroth, M. L.; LaTempa, T. J.; Grimes, C. A.; Desai, T. A. The Effect of TiO_2 Nanotubes on Endothelial Function and Smooth Muscle Proliferation. *Biomater.* **2009**, *30*, 1268–1272.
139. Grimes, C. A.; Mor, G. K. *TiO_2 Nanotube Arrays: Synthesis, Properties and Applications*; Springer: New York, 2009.
140. Roy, S. C.; Paulose, M.; Grimes, C. A. The Effect of TiO_2 Nanotubes in the Enhancement of Blood Clotting for the Control of Hemorrhage. *Biomater.* **2007**, *28*, 4667–4672.
141. Mor, G. K.; Carvalho, M. A.; Varghese, O. K.; Pishko, M. V.; Grimes, C. A. A Room Temperature TiO_2 Nanotube Hydrogen Sensor Able to Self-Clean Photoactively from Environmental Contamination. *J. Mater. Res.* **2004**, *19*, 628–634.
142. Salvador, P. Hole Diffusion Length in n-TiO_2 Single-Crystals and Sintered Electrodes—Photoelectrochemical Determination and Comparative Analysis. *J. Appl. Phys.* **1984**, *55*, 2977–2985.
143. Dloczik, L.; Ileperuma, O.; Lauermann, I.; Peter, L. M.; Ponomarev, E. A.; Redmond, G.; Shaw, N. J.; Uhlendorf, I. Dynamic Response of Dye-Sensitized Nanocrystalline Solar Cells: Characterization by Intensity-Modulated Photocurrent Spectroscopy. *J. Phys. Chem. B.* **1997**, *101*, 10281–10289.
144. Varghese, O. K.; Paulose, M.; Grimes, C. A. Long Vertically Aligned Titania Nanotubes on Transparent Conducting Oxide for Highly Efficient Solar Cells. *Nat. Nanotechnol.* **2009**, *4*, 592–597.
145. Paulose, M.; Peng, L.; Popat, K. C.; Varghese, O. K.; LaTempa, T. J.; Bao, N.; Desai, T. A.; Grimes, C. A. Fabrication of Mechanically Robust, Large Area, Polycrystalline Nanotubular/Porous TiO_2 Membranes. *J. Membr. Sci.* **2008**, *319*, 199–205.

146. Munoz, A. G. Semiconducting Properties of Self-Organized TiO_2 Nanotubes. *Electrochim. Acta* **2007**, *52*, 4167–4176.
147. Yu, K. P.; Yu, W. Y.; Ku, M. C.; Liou, Y. C.; Chien, S. H. Pt/Titania-Nanotube: A Potential Catalyst for CO_2 Adsorption and Hydrogenation. *Appl. Catal., B* **2008**, *84*, 112–118.
148. Linsebigler, A. L.; Lu, G.; Yates, J. T. Photocatalysis on TiO_2 Surfaces-Principles, Mechanisms, and Selected Results. *Chem. Rev.* **1995**, *95*, 735–758.
149. Tanaka, K.; Miyahara, K.; Toyoshima, I. Adsorption of CO_2 on TiO_2 and Pt/TiO_2 Studied by X-ray Photoelectron-Spectroscopy and Auger-Electron Spectroscopy. *J. Phys. Chem.* **1984**, *88*, 3504–3508.
150. Varghese, O. K.; Grimes, C. A. Appropriate Strategies for Determining the Photoconversion Efficiency of Water Photoelectrolysis Cells: A Review with Examples Using Titania Nanotube Array Photoanodes. *Sol. Energy Mater. Sol. Cells* **2008**, *92*, 374–384.
151. Koffyberg, F. P.; Benko, F. A. A Photoelectrochemical Determination of the Position of the Conduction and Valence Band Edges of p-Type CuO. *J. Appl. Phys.* **1982**, *53*, 1173–1176.
152. Nakaoka, K.; Ueyama, J.; Ogura, K. Photoelectrochemical Behavior of Electrodeposited CuO and Cu_2O Thin Films on Conducting Substrates. *J. Electrochem. Soc.* **2004**, *151*, C661–C665.
153. Lindgren, T.; Mwabora, J. M.; Avendano, E.; Jonsson, J.; Hoel, A.; Granqvist, C. G.; Lindquist, S. E. Photoelectrochemical and Optical Properties of Nitrogen Doped Titanium Dioxide Films Prepared by Reactive DC Magnetron Sputtering. *J. Phys. Chem. B* **2003**, *107*, 5709–5716.
154. Batzill, M.; Morales, E. H.; Diebold, U. Influence of Nitrogen Doping on the Defect Formation and Surface Properties of TiO_2 Rutile and Anatase. *Phys. Rev. Lett.* **2006**, *96*, 026103.
155. Henderson, M. A.; White, J. M.; Uetsuka, H.; Onishi, H. J. Photochemical Charge Transfer and Trapping at the Interface between an Organic Adlayer and an Oxide Semiconductor. *J. Am. Chem. Soc.* **2003**, *125*, 14974–14975.
156. Emeline, A. V.; Kuznetsov, V. N.; Rybchuk, V. K.; Serpone, N. Visible-Light-Active Titania Photocatalysts: The Case of N-Doped TiO_2—Properties and Some Fundamental Issues. *Int. J. Photoenergy* **2008**, 258394.
157. Torres, G. R.; Lindgren, T.; Lu, J.; Granqvist, C. G.; Lindquest, S. E. Photoelectrochemical Study of Nitrogen-Doped Titanium Dioxide for Water Oxidation. *J. Phys. Chem. B* **2004**, *108*, 5995–6003.
158. Wang, C.; Thompson, R. L.; Baltrus, J.; Matranga, C. Visible Light Photoreduction of CO_2 Using CdSe/Pt/TiO_2 Heterostructured Catalysts. *J. Phys. Chem. Lett.* **2010**, *1*, 48–53.